Catena 271 (2026) 110234

Contents lists available at ScienceDirect

Catena

journal homepage: www.elsevier.com/locate/catena

Traditional water meadows (*lameiros*) buffer the increase in sediment transport caused by recurrent fires in Mediterranean headwater basins

T. Bertocco [a,b,1,*], S.L. Santarén [b], T. de Figueiredo [a], R. Henriques [c], M. López-Vicente [d,1]

[a] CIMO, LA SusTEC, Instituto Politécnico de Bragança, Campus de Santa Apolónia, 5300253 Bragança, Portugal
[b] Grupo AQUATERRA, Centro Interdisciplinar de Química e Bioloxía (CICA-UDC), Universidade da Coruña, 15071 A Coruña, Spain
[c] Department of Earth Sciences, Institute of Earth Sciences (ICT), University of Minho (UMinho), Campus de Gualtar, 4710-057 Braga, Portugal
[d] GEOFOREST, Departamento de Ciencias Agrarias y del Medio Natural, Escuela Politécnica Superior de Huesca, Instituto de Investigación en Ciencias Ambientales (IUCA), Universidad de Zaragoza, 22071 Huesca, Spain

ARTICLE INFO

Dataset link: Shapefiles used for spatial analysis (Original data)

Keywords:
Sediment transport
Sediment connectivity
Lameiro
Forest fire
Burn severity
Recurrent fire
Headwater catchment

ABSTRACT

The role of traditional water meadows located at the valley bottom (*lameiros*) on the process of sediment transport remains poorly studied, especially after forest fires. We quantified the spatiotemporal changes of sediment transport caused by recurrent fires in two transboundary (N Portugal, NW Spain) headwater paired basins (32 km^2 in total) where tens of fires affected vegetation (Mediterranean forest) between 1997 and 2020. The difference Normalized Burn Ratio (dNBR), the Aggregated Index of sediment Connectivity (AIC), and the Sediment Delivery Ratio (SDR) were calculated for ten temporal scenarios, and how the 99 *lameiros* modulate the sedimentological response. Overall, 49.8% of the study area burned at least once, with low- to moderate-low severity prevailing, but higher recurrence, up to four times, affected northern and higher-altitude zones. Vegetation recovery and human activities (new forest trails, firebreaks and post-fire management) occurred unevenly across scenarios. The shorter the distance to *lameiros*, the lower fire severity and frequency. Over time, AIC and SDR increased with the largest fire-affected areas and slightly decreased with vegetation recovery. At the small sub-basin scale ($n = 756$; 549 burnt and 207 unburnt), *lameiros* reduced SDR by 36% and 7% in the burnt and unburnt sub-basins, respectively. Current soil erosion and sediment yield were of 3.34 and 3.96 Mg ha^{-1} yr^{-1}, and 322 and 344 Mg yr^{-1} in the two basins (calculated with RUSLE-AIC-SDR). Preservation, maintenance and restoration of *lameiros* should be prioritised as a nature-based and cost-effective solution that reduces fire propagation risk and soil loss.

1. Introduction

Forest fires represent a significant disturbance to soil properties (Agbeshie et al., 2022), and hydrological (Yu et al., 2019) and sedimentological dynamics, including increased runoff connectivity –mainly due to the loss of vegetation– (Fernández et al., 2020) at both immediate and long-term time scales (Vieira et al., 2018). In particular, soil erosion and sediment transport –including ash removal (Reneau et al., 2007)– reach exceptionally high rates in some areas, even surpassing erosive processes that have occurred over millennia (Ellett et al., 2019). In Mediterranean mountainous areas the impact of fire is accentuated owing to the combination of high temperatures and scarce precipitation in summer (Pausas and Vallejo, 1999) and, consequently, due to the slope of the terrain there are significant increases in sediment production (González-Romero et al., 2021). In Spain and Portugal, forest fires are a pressing threat, occurring frequently, destroying vast forest areas, but also bushland and suburban areas (Wilkinson et al., 2009). The year 2017 was challenging, with extensive fires occurring in both countries associated with abnormal droughts and heat waves. Portugal faced a particularly intense fire season, with a record total burnt area of approximately 500,000 ha (Editorial Nature Climate Change, 2017; Sánchez-Benítez et al., 2018). However, while the role of upslope vegetation loss in amplifying soil erosion and sediment transport is well documented, the specific contribution of valley-bottom wetland features, such as traditional water meadows, in modulating these dynamics under recurrent fire disturbance remains poorly understood.

* Corresponding author at: CIMO, LA SusTEC, Instituto Politécnico de Bragança, Campus de Santa Apolónia, 5300253 Bragança, Portugal
E-mail addresses: tamires.bertocco@ipb.pt (T. Bertocco), saul.leyva.santaren@udc.es (S.L. Santarén), tomasfig@ipb.pt (T. de Figueiredo), rhenriques@dct.uminho.pt (R. Henriques), manuel.lopezv@posta.unizar.es (M. López-Vicente).
[1] These authors contributed equally to this study.

https://doi.org/10.1016/j.catena.2026.110234
Received 2 December 2025; Received in revised form 5 May 2026; Accepted 11 May 2026
Available online 19 May 2026

Time series of maps are a powerful tool to track the impact of fires on sediment transport dynamics, capturing changes that have occurred in the vegetation (losses and gains), as well as post-fire practices (land use, actions on the ground, and topography), which modify the structure of the landscape (Colombaroli and Gavin, 2010; Martínez-Murillo and López-Vicente, 2018). On the other hand, assessing the severity of fires is fundamental to understanding the extent of the damage caused. For this assessment, indices derived from remote sensing (satellite and drone-derived imagery), such as the NBR (Normalized Burn Ratio) and dNBR (difference Normalized Burn Ratio) have been widely used to quantify the extent and intensity of the damage caused by fires (Neary et al., 2005; Alcaras et al., 2022). More recently, Miller and Thode (2007) proposed the relative dNBR (RdNBR), which stands out for providing more accurate assessments of fire severity in heterogeneous environments. Remote sensing tools such as the Google Earth Engine (GEE) allow efficient calculation of fire severity indices across large areas and time series (Vieira et al., 2023).

The sediment delivery ratio (SDR) is fundamental to understanding sediment transport in river basins (Abebe et al., 2023; López-Vicente et al., 2011). Essentially, SDR is the ratio between the sediment yield at the basin outlet and the average annual soil loss in its upstream area. This reflects the basin's capacity to send eroded sediment to its outlet (Liu, 1994; Wu et al., 2018). In parallel, the index of runoff and sediment connectivity (IC; Borselli et al., 2008), and its different versions –included the aggregated index of sediment connectivity (AIC; López-Vicente and Ben-Salem, 2019)–, is a useful computer-based tool to assess the spatial connection of sediments from their source area to a defined target (river, sink, lake, dam, outlet, etc.). Both, IC and AIC have been applied in a variety of topographic and land cover conditions and research contexts (Cavalli et al., 2013; Jin et al., 2024), including fire-affected areas (López-Vicente et al., 2020; van der Grift, 2021; Wu et al., 2021). Combining fire severity indices with the analysis of sediment connectivity is useful to understanding the response of these areas to disturbance events such as forest fires (Martínez-Murillo and López-Vicente, 2018; Martini et al., 2020). In the study of SDR, Vigiak et al. (2012) proposed the use of IC to estimate SDR for a large Australian basin. The combined use of IC and a soil erosion model (e.g. revised MMF) can be a suitable approach to derive maps of sediment trap effectiveness across the landscape (López-Vicente et al., 2015). Later, Hamel et al. (2015) designed the InVEST (Integrated Valuation of Environmental Services and Tradeoffs) set of tools, indicating the fate of eroded particles through SDR (Sharp et al., 2015; Ougougdal et al., 2020). The calculation of SDR in InVEST includes IC/AIC integration to understand better sediment transport processes (Hamel et al., 2015; Wu et al., 2025). This approach allows for a more complete analysis of soil erosion and sediment transport dynamics at different geographical scales, resulting in reliable and accurate estimates (Guo et al., 2023).

Lameiros (term in Portuguese and Galician) are traditional man-made irrigated grasslands occupying valley bottoms in the mountainous areas of NW Iberia. Unlike the surrounding heathland and shrubland, *lameiros* maintain dense herbaceous cover year-round due to irrigation and high soil moisture, which prevents fire ignition and spread (ICNF, 2020; Bertocco et al., 2025). Their valley-bottom position means they intercept the sediment pathways between slopes and stream channels, functioning as permanent sediment sinks that generate structural disconnectivity (Bertocco et al., 2025). While general vegetation cover is known to reduce post-fire erosion through temporal recovery, *lameiros* represent a persistent buffer whose effectiveness is independent of fire-induced vegetation loss. This distinction has not yet been explored in post-fire sediment connectivity research. Moreover, the progressive abandonment of these meadows threatens both their hydrological function and their role as natural firebreaks, yet the geomorphological consequences of this abandonment under recurrent fire regimes remain unquantified. In Portugal, active *lameiros* are officially recognised by the ICNF (Institute of Nature and Forest Conservation) as structural elements of wildfire prevention (ICNF, 2020).

Until now, no study has yet assessed how *lameiros* modulate the spatiotemporal response of sediment connectivity and SDR under recurrent fire regimes. Existing studies on vegetation-mediated buffering of post-fire sediment transport focus on upslope vegetation recovery dynamics (Shakesby, 2011; López-Vicente et al., 2021) but neglect the role of permanent valley-bottom wetland features as structural disconnectors. This study addresses three key scientific questions: (i) How do recurrent fires modify sediment connectivity and SDR over a multi-decadal period in headwater Mediterranean basins? (ii) Do *lameiros* effectively buffer sediment delivery increases caused by fire, and does their buffering function differ quantitatively from that of general vegetation cover? and (iii) Does the spatial proximity and use status of *lameiros* influence fire severity and recurrence? To achieve this goal, the maps of AIC and SDR, all dimensionless, are generated for 10 temporal scenarios in a 24-year period (from 1997 to 2020) by means of integrating high-quality and reliable input data obtained or generated from distinct and independent sources. This study does not aim to quantify the exact amount of exported sediment over the analyzed period, but to evaluate the temporal dynamic of sediment transport potential in basins affected by recurrent fires and subjected to opposite land cover changes (vegetation loss due to fires and gain due to recovery). Finally, we estimate soil erosion and sediment yield for the most recent scenario as an order-of-magnitude reference to support a soil conservation proposal with a special focus on *lameiros*.

2. Materials and methods

2.1. Study area

Two paired basins located in the transboundary zone between Spain and Portugal were delimited: 'Ribeira de Candanedos' basin ('B.08'; 14.5 km^2) and 'Ribeira do Sil' basin ('B.13'; 17.2 km^2), which outlets come together in the same point that is the beginning of Igrejas River (Fig. 1a, b). The entire surface located in Portugal is under environmental protection, being part of the Natural Park of Montesinho. In a previous recent study, all *lameiros* were accurately mapped (n = 99), with 51 located in basin B.08 and 48 in basin B.13. Their areas estimated with mean values of 3056 and 4438 m^2 in B.08 and B.13) (Bertocco et al., 2025) (Fig. 1c). The topography of the basins is characterized by undulating terrain with moderate to high average slopes ($\overline{S}$=21% and 20% in B.08 and B.13). The permanent streams in the main valleys cross the basins from north to south.

The region's climate is temperate Mediterranean with continental influence, with distinct seasons, including a wet period from October to February and a dry summer with low rainfall in July and August. The average annual temperature and precipitation is 12.1 °C and 733 mm. The predominant vegetation includes heathland and moorland, coniferous forests, transitional woodland shrubs, and areas of sparse vegetation. Small-scale agricultural mosaics, including some cereals, pastures, and dispersed orchards (e.g. olive groves and vineyards), interspersed with natural and semi-natural areas, occupy only about 1%. Man-made linear landscape elements (e.g. forest trails, firebreaks, and paved mountainous road) occupy less than 2%. According to de Figueiredo (2013), shales, which is the predominant lithology, give rise to poorly developed soils with high stoniness, such as Leptosols and Cambisols (Bertocco, 2021). Leptosols, which are shallow and common in areas with steep slopes, facilitate surface runoff (Afonso and Arrobas, 2009), while Cambisols, which are deeper, have greater infiltration capacity (de Figueiredo, 2013). All variables and parameters used in the models are listed in Table 1 for reference.

2.2. Study period and forest fires

A 24-year period was defined to study the impact of fires and recurrent fires on sediment connectivity and transport at medium-term.

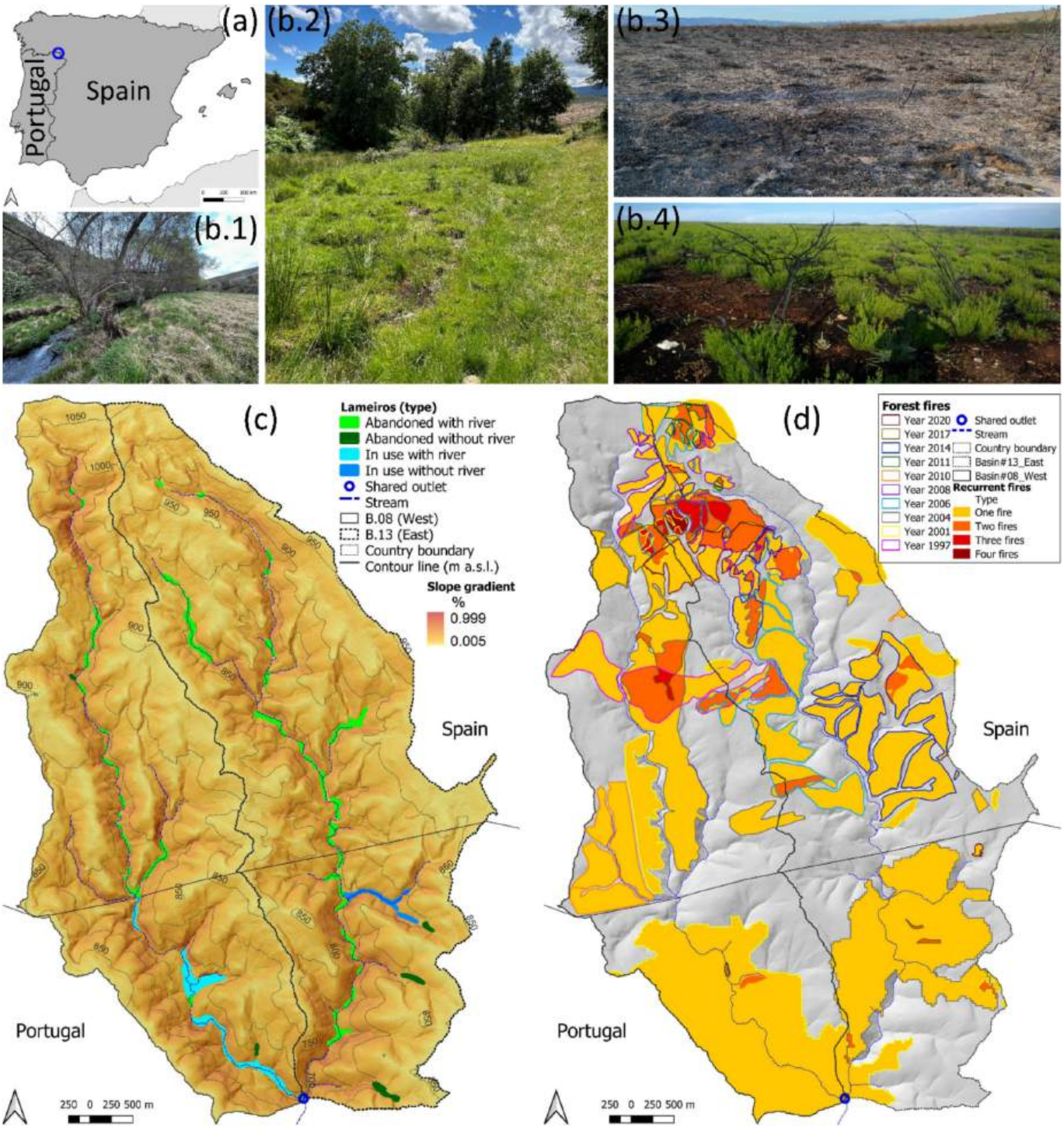

Fig. 1. Location of the study area (blue circle) between Spain and Portugal (a), and pictures of the landscape showing the *lameiros* with (b.1) and without river (b.2); and a fire-affected area just after the fire (b.3) and with vegetation regrowth (b.4). Hillshade-map derived from the DEM including the location of the four types of *lameiros*, the slope gradient map, the contour lines of elevation and the stream network used as computational target of sediment connectivity (c), and location and extension of the burnt areas –including recurrent fires– during the 24-year study period (d). (For interpretation of the references to colour in this figure legend, the reader is referred to the web version of this article.)

Using high-resolution (between 0.25 × 0.25 m and 1 × 1 m; in most cases of 0.5 × 0.5 m) aerial orthophotos (PNOA series of the Spanish National Center of Geographic Information - CNIG), ten representative past scenarios (SC), which correspond to specific dates and temporal settings, were defined to simulate sediment connectivity and transport, namely: October 1997 (reference year, SC1), August 2001 (SC2), July 2004 (SC3), August 2006 (SC4), July 2008 (SC5), July 2010 (SC6), July 2011 (SC7), July 2014 (SC8), July 2017 (SC9) and August 2020 (SC10) (Table 2). Using the previous scenario as basis for the comparison, the observed changes between each pair of consecutive scenarios were assessed: ΔSC2–1, ΔSC3–2, ΔSC4–3, ΔSC5–4, ΔSC6–5, ΔSC7–6, ΔSC8–7, ΔSC9–8, ΔSC10–9, and finally ΔSC10–1 for the complete series.

One hundred eight fires affected the study area and its surroundings

Table 1
Variables and parameters used throughout this study.

Symbol	Description	Units
A	Upslope drainage area	m^2
AIC	Aggregated Index of sediment Connectivity	Dimensionless ($-\infty$, $+\infty$)
AIC_0	AIC calibration parameter	dimensionless
AWC	Aggregated weighting factor	dimensionless
C	Vegetation and management factor	Dimensionless (0–1)
C_t	Vegetation and management factor (C-RUSLE, normalized)	dimensionless (0.001–1)
D_{dn}	Probability of runoff and sediment reaching a sink along the flow path	dimensionless
d_i	Flow path distance at each pixel	m
$dNBR$	Difference Normalized Burn Ratio	dimensionless
Dup	Upstream component	dimensionless
E	Soil erosion	Mg ha^{-1} yr^{-1}
$EI30$	Monthly rainfall erosivity	MJ mm ha^{-1} h^{-1} $month^{-1}$
K	Soil erodibility factor	Mg h MJ^{-1} mm^{-1}
K_b	SDR shape parameter	dimensionless
K_p	Soil permeability factor	dimensionless (0.001–1)
LS	Slope length and gradient factor	dimensionless
M	Soil texture parameter (silt + fine sand)	%
NBR	Normalized Burn Ratio	dimensionless
NIR	Near infrared band reflectance	dimensionless
OM	Organic matter content	%
P	Soil conservation factor	Dimensionless (0–1)
R	Rainfall erosivity factor	MJ mm ha^{-1} h^{-1} yr^{-1}
R_t	Normalized rainfall erosivity factor	dimensionless (0.001–1)
RT	Terrain roughness factor	dimensionless (0.001–1)
S	Slope gradient	dimensionless (0.001–1)
SDR	Sediment Delivery Ratio	Dimensionless (0–1)
SDR_{max}	Maximum SDR value	Dimensionless (0–1)
SSY	Area-specific sediment yield	Mg ha^{-1} yr^{-1}
$SWIR$	Shortwave infrared band reflectance	dimensionless
SY	Sediment yield	Mg yr^{-1}

during the study period (mean rate of 4.5 fires per year). None of these fires covered the whole surface of the two basins, being small fires in most cases: 1 fire in 1997, 1 fire in 1998, 3 fires in 1999, 15 fires in 2001, 17 in 2002, 10 in 2003, 12 in 2004, 9 in 2005, 6 in 2006, 5 in 2007, 11 in 2008, 1 in 2009, 3 in 2010, 1 in 2011, 8 in 2012, 4 in 2015, 1 in 2016, 1 in 2017, and 1 in 2020 (Table 2). These fires were distributed across various years, with the majority occurring between 2001 and 2008, a period of significant fire activity in the region (ca. 12 fires per year). Note that the official fire databases were used solely for temporal characterization of fire occurrence (dates, causes, and number of fires). The spatial quantification of burned areas within each basin, including the breakdown by scenario, was performed using the high-resolution aerial orthophotos (PNOA series), as described below (steps I-VI), since the official records do not provide spatially explicit fire perimeters compatible with the basin boundaries.

The data used in this analysis come from two primary sources: The Spanish *Ministerio de Agricultura, Pesca y Alimentación* (MAPA) and the Portuguese *Instituto da Conservação da Natureza e Florestas* (ICNF). Both sources provided crucial information such as each fire's date, cause, burned area, and geographical coordinates. For Spain, data were meticulously extracted from the *Estadística General de Incendios Forestales* (EGIF), a dataset compiled by the *Coordinación de la Información Nacional de Incendios Forestales* (CINIF), covering the period 1968–2021. In Portugal, fire data were retrieved from the ICNF's *Sistema de Gestão de Informação de Incêndios Florestais* (SGIF) for the period 2001–2023. However, data from 1980 to 2000 were only available at the municipal level, lacking precise geographical coordinates. For this earlier period, geographical estimates were made based on the locations of the municipalities to evaluate whether the fires impacted the study area.

In both countries, the mapped fire areas were cross-referenced with spatial data in a thorough and meticulous process to assess fire distribution and recurrence over time. The majority of fires, 85%, were intentional. Fires caused by accidents or negligence accounted for 3.7%, while 0.93% were linked to campfires. Fires started by lightning represented 0.93% of the total, and 6.5% of fires had an unknown cause. Lastly, 2.8% were attributed to re-ignition of previous fires. These classifications provide valuable insights into the causes of fires in the region (Supplementary Table 1).

In a first step and using the orthophotos, the following layers were mapped for each scenario: I) areas where fires occurred (loss of vegetation) –further used for the burn severity assessment–; II) areas with recovery/ gain of vegetation; III) construction of new forest roads; IV) abandonment of forest roads; V) opening of new firebreaks; and VI) abandonment of firebreaks. This task allowed us to quantify the real area affected by fires and the extent of the area affected by recurrent fires throughout the study period (Fig. 1d).

2.3. Burn severity assessment

Burn severity was mapped using the Normalized Burn Ratio (NBR) and the differentiated Normalized Burn Ratio (dNBR) (Key and Benson, 2006). NBR (Eq. 1) calculates the distant responses of the near infrared (NIR: 0.64–0.67 mm) and shortwave infrared (SWIR: 1.57–1.65 mm) bands, making it possible to discern between areas of intact vegetation and burnt surfaces:

$$NBR = (NIR - SWIR)/(NIR + SWIR) \quad (1)$$

NBR returns values between −1 and 1. Healthy green vegetation will have a high NBR value while burnt vegetation will have a low value. Areas of dry, brown vegetation or bare soil will also return lower NBR values than green vegetation. dNBR is calculated by the difference between the post-fire and pre-fire NBR values (Eq. 2), and then used to calculate the scaled burn severity index:

$$dNBR = NBR_{pre-fire} - NBR_{post-fire} \quad (2)$$

The dNBR value can be more useful than the NBR alone to determine what is burnt as it shows change from the baseline state. A burnt area will have a positive dNBR value while an unburnt area will have a negative dNBR value or a value close to zero. dNBR can also be used to describe burn severity. A higher severity fire will burn more vegetation, resulting in a higher dNBR. Rahman et al. (2018) found –using Sentinel-2 imagery– that the dNBR threshold values for differentiating burnt from unburnt areas may change in areas with different vegetation types. In this study, we used the burn severity classes based on dNBR values as outlined by Key and Benson (2006) (Table 4).

Unburned areas potentially show an increase in vegetation due to growth. Low severity areas are characterized by light damage to vegetation and soil, which allows for rapid recovery. Moderate-low severity refers to areas with more evident fire damage, where vegetation is partially lost but some plants survive. Moderate-high severity areas experience significant damage, affecting most vegetation, resulting in a slower recovery (Fig. 1b). Finally, high severity represents areas where almost all vegetation is destroyed, leading to exposed soil and a significantly altered landscape. The use of burn severity classes was limited to the areas where vegetation loss was previously identified by using the high resolution aerial orthophotos. In previous studies conducted in Mediterranean fire-affected areas, covering Spain (López-Vicente et al., 2020; García-Llamas et al., 2020), Portugal (Follmi et al., 2022), and in regions encompassing both countries (Häusler et al., 2018), the use of burn severity maps to refine the parameterization of the C-RUSLE factor was an initial step before proceeding to calculate soil erosion and/or sediment connectivity/ transport. The C-RUSLE factor is the vegetation and cultivation management factor defined in the RUSLE model of soil erosion (Renard et al., 1994).

Table 2
Simulated scenarios and data sources used to characterize the forest fires and generate the land use and land cover maps. The number of fires that affected the study area and/or the surrounding areas between each pair of scenarios are also indicated.

Date	Fires	Scenario	Land use and land cover map data source					Satellite imagery	
Year	number	Name	PNOA	SIOSE (SP)	COS (PT)	ICNF (PT)	FIRE (SP)	Pre-fire	Post-fire
1995	–								
1996	–					Yes			
1997	1	Sc1	10/1997	2005	1995			Sc1: 09/02/1997 (L5)	Sc1: 05/09/1997 (L5)
1998	1					Yes			
1999	3					Yes		Sc2: 15/02/1999 (L5)	
2000	0								
2001	9	Sc2	07/08/2001	2005	1995				Sc2: 07/08/2001 (L7)
2001	6							Sc3: 03/11/2001 (L5)	
2002	17						Yes		
2003	10					Yes			
2004	12	Sc3	25/07/2004	2005	2007		Yes		Sc3: 07/08/2004 (L5)
2005	8							Sc4: 30/01/2005 (L5)	
2006	5	Sc4	12/08/2006	2005	2007		Yes		Sc4: 12/07/2006 (L5)
2006	1							Sc5: 12/07/2006 (L5)	
2007	5								
2008	11	Sc5	18/07/2008	2009	2007		Yes		Sc5: 17/07/2008 (L5)
2009	1							Sc6: 06/09/2009 (L5)	
2010	0	Sc6	25/07/2010	2009	2010		Yes		Sc6: 24/08/2010 (L5)
2010	3							Sc7: 24/08/2010 (L5)	
2011	1	Sc7	20/07/2011	2011	2010		Yes		Sc7: 26/07/2011 (L5)
2011	0							Sc8: 14/10/2011 (L5)	
2012	8								
2013	0								
2014	0	Sc8	30/07/2014	2014	2015		Yes		Sc8: 16/06/2014 (L8)
2014	0							Sc9: 16/06/2014 (L8)	
2015	4								
2016	1								
2017	1	Sc9	02/07/2017	2017	2018		Yes		Sc9: 26/07/2017 (L8)
2018	0							Sc10: 01/10/2018 (L8)	
2019	0								
2020	1	Sc10	22/08/2020	2017	2018		Yes		Sc10: 04/09/2020 (L8)

PNOA: aerial orthophoto; SIOSE (SP): land use and land cover map of Spain; COS (PT): land use and land cover map of Portugal; ICNF (PT): forest fire information from Portugal; FIRE (SP): forest fire information from Spain; L5: Landsat 5; L7: Landsat 7; L8: Landsat 8.

2.4. Satellite imagery acquisition and processing

Google Earth Engine (GEE) platform, based on a JavaScript programming environment, was used for free acquiring, processing, and analyzing time series images. One of the main advantages of GEE lies in its ability to perform analyses and interpretations in parallel, resulting in more agile processing of extensive geospatial data sets over long time series, overcoming the limitations of conventional computing resources (Long et al., 2019; Amani et al., 2020).

The Landsat satellite images were acquired from the United States Geological Survey (USGS) archive and were available on GEE (Application Programming Interface v.0.1.405; Geemap library v.0.32.1). For the specific period of this study, images from Landsat 5 ($n = 14$ images), Landsat 7 (n = 1) and Landsat 8 ($n = 5$) were used. These satellite images are from Level 2, Collection 2, Tier 1. All these images have a pixel size of 30 × 30 m. For Landsat 5 and 7, the band corresponding to the NIR is SR_B4, and the one for the SWIR is SR_B7, while for Landsat 8, NIR is SR_B5, and SWIR remains the same (SR_B7). The optical bands of each of these images were multiplied by a scale factor of 2.75e-5 and were added an offset of −0.20, to transform the data into reflectance units. Two images, one pre-fire and one post-fire, were selected for each scenario, following this criteria: I) the pre-fire image is the first image prior to the date of the orthophoto (from PNOA) of the corresponding scenario in which the new fire observed in the orthophoto cannot be seen (ruling out old burned areas); and II) the post-fire image is the satellite image closest in time (before or after) to the date of the orthophoto of the corresponding scenario in which the same fires racteristic of the corresponding scenario can be seen (Table 2). All images were preview using Google Colab. To ensure data quality, we only selected images with low cloud cover (average cloud cover of 1.5% from the 20 images; Supplementary Table 2). The calculations of NBR and dNBR were also performed in GEE for visualization and subsequent download.

2.5. Sediment connectivity: Index, inputs and configuration

The aggregated index of sediment connectivity (AIC) offers a comprehensive approach to assessing sediment connectivity at different spatial and temporal scales (López-Vicente et al., 2020; Wu et al., 2023), including mountain areas affected by forest fires (van der Grift, 2021). The AIC metric combines the downstream potential for upstream flow direction (D_{up} component) and the probability of runoff and sediment reaching a sink along the flow path (D_{dn} component):

$$AIC_k = log_{10}\left(\frac{D_{up,k}}{D_{dn,k}}\right) = log_{10}\left(\frac{\overline{R_t} \bullet \overline{RT} \bullet \overline{C_t} \bullet \overline{K_P} \bullet \overline{S} \bullet \sqrt{A_k}}{\sum_{k=i}^{n} \frac{d_i}{AWC_i}}\right) \quad (3)$$

$$AWC_i = R_{ti} \bullet RT_i \bullet C_{ti} \bullet K_{Pi} \bullet S_i \quad (4)$$

The subscripts $\boldsymbol{k}$ and $\boldsymbol{n}$ indicate that each cell has its own AIC-value and the total number of pixels that sediment travels from its source area to the defined target, respectively. All inputs, except $\boldsymbol{A}$, have normalized dimensionless values between 0.001 or 0.005 and 1 (López-Vicente et al., 2021). The values in the $\boldsymbol{D_{up}}$ component correspond to the average values of the upstream drainage area in each pixel. AIC index is defined in the range $[-\infty, +\infty]$, and higher AIC values indicate higher degrees of connectivity. Index configuration affect output maps and values because IC and AIC depend on the computational target (Cavalli et al., 2013; López-Vicente et al., 2020). In this study, sediment connectivity was associated with the average stream conditions –avoiding summer low

water and winter floods– that were analyzed in detail by Bertocco et al. (2025) (Fig. 1c). The choice of the stream network as computational target is justified because watercourses are permanent features, and longitudinal sediment connectivity within them is an actual fact. As *lameiros* are located within or adjacent to the stream network, their buffering effect is effectively captured in this configuration. It should be noted that a different computational target (e.g., the basin outlet) would likely yield different SDR values and reduction percentages. All inputs and outputs were processed at a 5 × 5 m resolution using cartographic tools such as weighted flow length and flow accumulation, employing the Deterministic Infinity (D-Inf) algorithm in QGIS Desktop 3.26.3 and ArcGIS Pro 3.1.2.

The AIC uses the following input factors: $\boldsymbol{R_t}$ is the normalized rainfall erosivity factor, $\boldsymbol{RT}$ represents the roughness of the terrain, $\boldsymbol{C_t}$ is the vegetation and cultivation management factor (C-RUSLE), $\boldsymbol{K}_p$ is the soil permeability factor, $\boldsymbol{S}$ is the slope gradient, $\boldsymbol{A}$ is the upslope drainage area (m^2), $\boldsymbol{d_i}$ is the distance of the flow path at each pixel (m), and $\boldsymbol{AWC}$ is the aggregated weighting factor. The subscript $\boldsymbol{t}$ refers to the user-defined period of each simulation, that corresponded to each scenario in this study. The rainfall erosivity factor map was generated using the information from the three weather stations (WS) that surround the study area: one in Spain called 'Puebla de Sanabria' WS (42° 03′ 30.0312" N, 6° 37' 49.5194" W; data source: Duero River Water Authorities), and two in Portugal called 'Rio de Onor' WS (41° 56′ 14.7" N, 6° 37' 5.2" W) and 'Montezinho' WS (41° 55′ 55.2" N, 6° 47' 6.0" W). The data of the two WS located in Portugal were obtained from the National Water Resources Information System (SNIRH) database. To estimate the rainfall erosivity factor at annual ($\boldsymbol{R}$; MJ mm ha^{-1} h^{-1} yr^{-1}) and monthly ($\boldsymbol{EI30}$; MJ mm ha^{-1} h^{-1} $month^{-1}$) scales, data from 9 hydrological years were used: from 2015 to 2023. $\boldsymbol{EI30}$ was calculated for each month of each year, and then averaged across the 9-year period to obtain monthly values; $\boldsymbol{R}$ was obtained by summing the 12 monthly $\boldsymbol{EI30}$ values. This period is defined by the availability of data from the three WSs; records prior to 2015 are limited and have many gaps. The approach developed by de Santos Loureiro and de Azevedo Coutinho (2001) in Portugal was employed to estimate $\boldsymbol{R}$ using daily rainfall depth values, a method that has been successfully tested in different countries like Italy, Spain, Poland or Vietnam, among others (Diodato, 2004; López-Vicente et al., 2011; Ranzi et al., 2012; Halecki et al., 2018). The formula used for calculating $\boldsymbol{R}$ is as follows:

$$R = \frac{1}{N}\sum_{m=1}^{12}\left(7.05 \bullet rain_{10} - 88.92 \bullet days_{10}\right) \quad (5)$$

where $\boldsymbol{N}$ is the number of years, $\boldsymbol{m}$ is the month, $\boldsymbol{rain_{10}}$ is the monthly rainfall ≥10 mm, and $\boldsymbol{days_{10}}$ is the number of days per month with rainfall ≥10 mm. Once the calculation of the R factor for each WS was completed, a map was generated by interpolation, with the technique Spline (type: Tension, weight = 100). The rainfall erosivity map was treated as a structural variable with only spatial variability and non-temporal change. This approach was adopted due to the limited availability of precipitation data prior to 2015, with records prior to 2003 being unavailable for the three surrounding weather stations. The 9-year record used is consistent with the minimum requirements of the European literature, where records as short as 5 years have been accepted for R-factor calculation (Panagos et al., 2015a), although this approach may underestimate actual sediment yield during years with extreme rainfall events. Since the same $\boldsymbol{R}$ map was applied consistently to all ten scenarios, the relative comparisons between scenarios remain robust.

The topographic (RT, S, A) and edaphic (Kp) inputs were adopted from the previous study made by Bertocco et al. (2025). A detailed and accurate land use and land cover (LULC) map was generated for each scenario by combining information from various sources (Fig. 2), namely: The Spanish Land Use Information System (SIOSE) with vector maps corresponding to the years 2005, 2009, 2011, 2014 and 2017; and the Portuguese Land Use and Occupation Map (COS) with maps for the years 1995, 2007, 2010, 2015 and 2018. After combining these data sources, the linear landscape elements (paved roads, forest trails and firebreaks) and fire-affected areas where included. This integration of multiple sources and years allowed for creating detailed and representative maps, supporting a comprehensive analysis of the temporal dynamics. We also generated the map of land uses before Sc1, which was called scenario zero (Sc0), including 606 polygons and 79 land uses (Fig. 2a; Supplementary Table 3). Sc0 presented a landscape dominated by resident vegetation, with a significant presence of shrubland and pastures (48% of the total area), complemented by transitional areas (19%; scattered shrubs and trees) and coniferous forests (12%), reflecting the natural vegetation before the fires. Natural pastures covered about 9%, while 7% of the area was covered by sparse vegetation (disperse shrubs and herbs). The remaining area (5%) consisted of rainfed cultivated areas, paved surfaces, and bodies of water (streams).

For all scenarios, the C-RUSLE values were calculated from those proposed by Panagos et al. (2015a) for European Union countries and by Marques et al. (2021) specifically for Portugal. For those areas affected by fires and subjected to vegetation recovery, we used the studies made by Fernandez-Manso et al. (2016) and López-Vicente et al. (2021) in burnt Mediterranean areas with vegetation regrowth, to stablish five temporal ranges: 1–2 years, 3–4 years, 5–7 years, 8–14 years, and 15 or more years (regenerated to pre-fire vegetation), as detailed in Supplementary Table 4. Therefore, ten maps of land use and land cover were generated, including all the information of the burnt areas and those with vegetation recovery.

2.6. Sediment delivery ratio: Spatially distributed approach

The SDR was calculated for the ten scenarios as a function of the Aggregated Index of Sediment Connectivity (AIC), using the formula originally proposed by Vigiak et al. (2012):

$$SDR_i = SDR_{max} \Big/ 1 + \exp\left(\frac{AIC_{0i} - AIC_i}{K_b}\right) \quad (6)$$

where $\boldsymbol{SDR_{max}}$ is the maximum SDR value for the study area, and $\boldsymbol{AIC_0}$ and $\boldsymbol{K_b}$ are calibration parameters. In those basins where records of sediment yield are available (e.g. from a gauging station), the $\boldsymbol{AIC_0}$ and $\boldsymbol{K_b}$ parameters can be adjusted to the specific characteristics of the basin and for specific rainfall-runoff events (Hamel et al., 2015). As this data are not available in our study area, we used the default values typically set in the literature (in Finland (Räsänen et al., 2024), China (Qiao et al., 2024), Australia (Yang et al., 2024) and Spain (Abebe et al., 2023)): $\boldsymbol{AIC_0} = 0.5$ and $\boldsymbol{K_b} = 2.0$.

The $\boldsymbol{SDR_{max}}$ mainly depends on the basin size, with values close to 1 for small basins (< 100 km^2) affected by heavy soil water erosion without sedimentation-prone features in the landscape, to 0.80 or 0.70 for large (ca. 100,000 km^2) and very large (>1 × 10^6 km^2) basins, respectively, where intra-basin sedimentation happens due to natural (geomorphology) and/or anthropogenic (e.g. dams) causes (Lu et al., 2006). In a previous study done in the same basins of this study, Bertocco et al. (2025) found that the 99 *lameiros* located in the bottom valley of the stream network act as sedimentation-prone areas during most part of the year generating areas of partial dis-connectivity. Therefore, we set $\boldsymbol{SDR_{max}} = 0.90$.

2.7. Current soil erosion and sediment yield

For the most recent scenario (year 2020), sediment yield ($\boldsymbol{SY_B}$; Mg yr^{-1}) and area specific sediment yield ($\boldsymbol{SSY_B}$; Mg ha^{-1} yr^{-1}) were calculated for the two basins by coupling the RUSLE model of soil loss ($\boldsymbol{E}$; Mg ha^{-1} yr^{-1}) and the AIC-SDR approach of sediment transport of that scenario:

$$SSY_{Bi} = E_i \cdot SDR_i \quad (7)$$

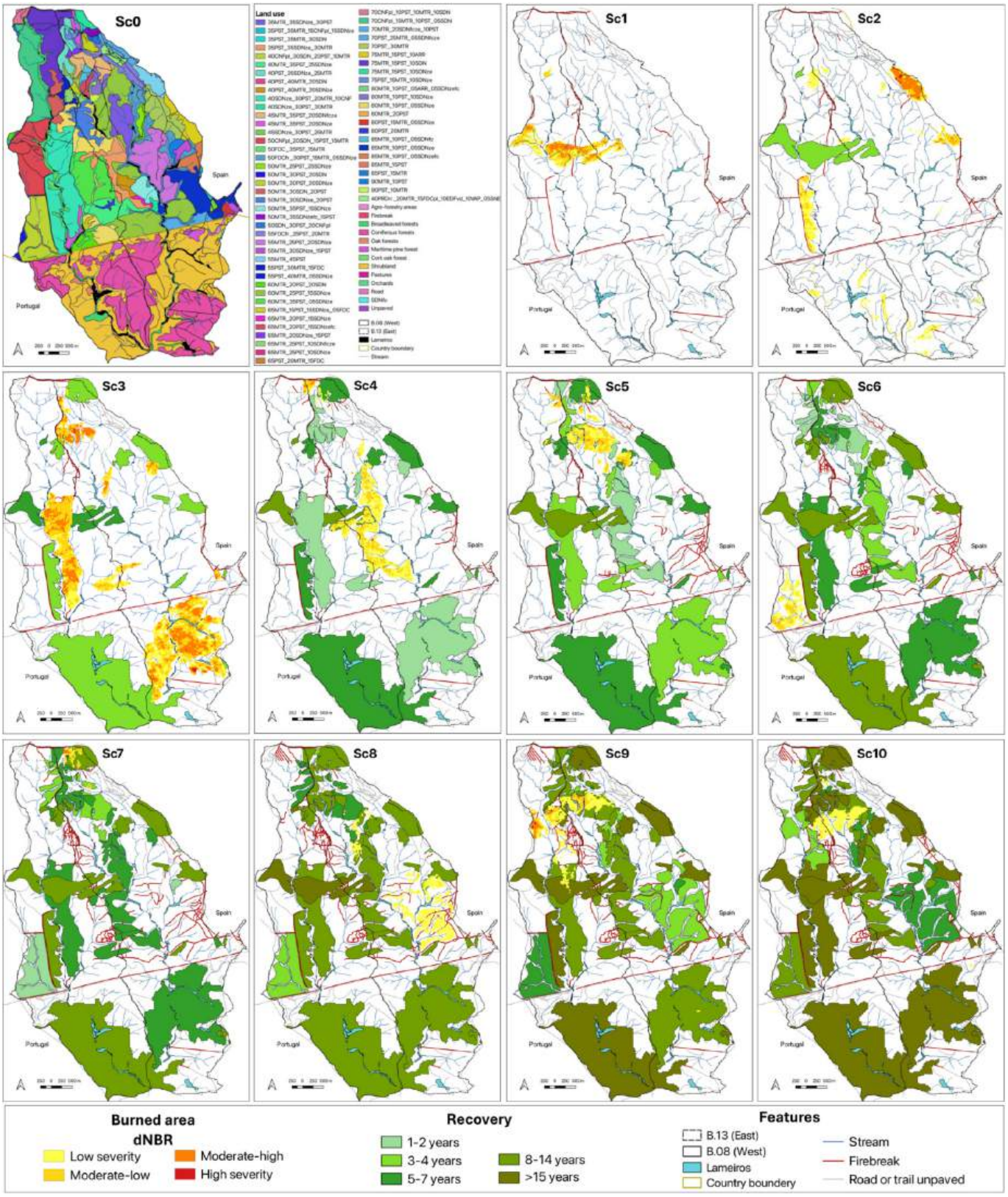

Fig. 2. Map of land uses before the 24-year period of study (Sc0; see Supplementary Table 3), and evolution (from Sc1 to Sc10) of the fire-affected areas and those with vegetation recovery at each scenario. The severity of the fire is included as well as the level of vegetation recovery, the rivers (dark blue lines) and *lameiros* (blue polygons). (For interpretation of the references to colour in this figure legend, the reader is referred to the web version of this article.)

$$SY_B = \left(\sum_{i=1}^{N} (E_i \bullet SDR_i) \right) \cdot (25/10000) \quad (8)$$

$$E_i = R_i \cdot K_i \cdot LS_i \cdot C_i \cdot P_i \quad (9)$$

where $\boldsymbol{N}$ represents the total number of pixels $\boldsymbol{i}$ at each basin $\boldsymbol{B}$. $\boldsymbol{E_i}$ was calculated following the approach of Renard et al. (1994) as a function of rainfall erosivity ($\boldsymbol{R}$; MJ mm / ha h yr), soil erodibility ($\boldsymbol{K}$; Mg h / MJ mm), the vegetation and management factor ($\boldsymbol{C}$; dimensionless, between 0 and 1), the slope length and gradient factor ($\boldsymbol{LS}$; dimensionless), and the soil conservation factor ($\boldsymbol{P}$; dimensionless, between 0 and 1). The generated map of soil erosion ($\boldsymbol{E_i}$) was corrected by means of removing the values of $\boldsymbol{E_i}$ in those pixels that correspond to the two rivers (with the same mask previously used for the configuration of AIC). This correction aimed to avoid the mistake of considering the sediments stored within the rivers as soil particles from the slopes.

Soil erodibility is a complex property ($\boldsymbol{K}$)was calculated following Renard et al., 1997 using soil samples collected in the field (Supplementary Table 5):

$$K = \frac{\left[2.1 \cdot 10^{-4} (12 - OM) M^{1.14} + 3.25(s-2) + 2.5(p-3)\right]}{100} 0.1317 \quad (10)$$

$$M = (silt + fine\ sand)^*(100 - clay) \quad (11)$$

The $\boldsymbol{LS}$-factor map was generated following the approach of Desmet and Govers (1996) that is implemented in SAGA GIS 9.7.1 and using the multiple flow accumulation algorithm. This option was selected as the appropriate one by the European Soil Data Centre (ESDAC) of the European Commission (Panagos et al., 2015b). No agricultural terrace appears in our study area, and *lameiros* are the only man-made structure that retains sediments and reduces overland flow velocity. Based on the characteristic of this unique land use, with dense grass vegetation covering the whole surface throughout the year, and moderate slope gradient (11.3% and 13.3% in B.08 and B.13), and on the literature (Panagos et al. (2015c) made a review study of the different components of the P-factor for 28 European countries), we proposed a $\boldsymbol{P}$-factor value for *lameiros* equals to 0.853.

2.8. Spatial analysis and role of lameiros on fire propagation, sediment delivery and soil loss

In order to shed light to the factors that explain the occurrence of fires, a spatial analysis was done considering four fire parameters (location and extension of the burnt areas, average fire severity, and fire recurrence) for each temporal scenario, and six physiographic parameters (elevation, topographic aspect, slope gradient, density of vegetation, distance to the *lameiros*, and distance to the trails and firebreaks). Among these parameters, distance to *lameiros* was specifically included to assess the spatial influence of these features on fire occurrence, severity and recurrence. This cross-spatial analysis was conducted using GIS tools available in QGIS Desktop 3.40.1. Values of altitude, slope gradient and vegetation cover density (represented by the C-RUSLE factor) were classified into ten intervals, whereas slope orientation into eight classes (N, NE, E, SE, S, SW, W, and NW), and distance to *lameiros* and distance to trails and firebreaks into four intervals (5, 20, 50 and 100 m). Regarding fire parameters, occurrence refers to the presence or absence of fire in each class, indicating whether burned areas were recorded within that class in each scenario. The extent corresponds to the average burned area per physiographic class, expressed in hectares. The severity of the burned areas was estimated using the dNBR index, considering areas with dNBR values $\geq$0.1 as severe. Finally, recurrence was quantified as the maximum number of times the same area was affected by fires during the analyzed period.

The evolution in the values of sediment connectivity was done by mapping the areas with the highest (> percentile 90: P90), lowest (< P10) and moderate (> P40 - < P60) values of AIC of the ten scenarios. This analysis considered each basin independently. Persistent areas with P10, P40-P60 and P90 values were identified, considering the location of *lameiros* and the burnt areas, and the influence of areas with recurrent fires. For the SDR, the analysis was performed based on mapping its evolution across the ten scenarios, evaluating the relationship between SDR patterns, burned areas, and the location of *lameiros*. A graph was also prepared to display the mean SDR values obtained in each scenario, facilitating a quantitative comparison between the results. The values of soil erosion and SSY obtained for the most recent scenario were evaluated in terms of land uses, in order to identify those areas with very low, low, moderate, high and very high rates of soil loss taking into account the value of tolerable soil loss (2 Mg ha^{-1} yr^{-1}; ESDAC, 2020) and the generally accepted soil formation rates in Europe (1.4 Mg ha^{-1} yr^{-1}; Verheijen et al., 2009).

The validation of model and indices predictions at ungauged basins is a complex task with limitations. Swarnkar et al. (2018) determined for a headwater basin that the uncertainties in soil erosion and sediment transport and yield estimates with RUSLE and SDR depended on the uncertainties of inputs, especially on the spatial propagation of the uncertainties of the C and LS factors. In our study, all inputs were prepared with detail, compiling data from several rigorous sources in order to minimize the spatial uncertainties of the information. On the other hand, the good prediction ability of IC and AIC was demonstrated in other Mediterranean fire-affected areas where post-fire practices include the installation of small barriers in the hillslopes or check-dams in the areas where overland flow is concentrated and sediment transport was calculated with field measurements (Martínez-Murillo and López-Vicente, 2018; González-Romero et al., 2021). In Portugal, only a small number of river basins are equipped with monitoring stations capable of measuring sediment yield or overland flow turbidity. Most existing stations are instead dedicated to **water-quality monitoring, hydrometric measurements** (e.g., streamflow and water level), and **meteorological observations** (e.g., precipitation and wind) (data source: *Serviço Nacional de Informação em Recursos Hídricos*, https://snirh.apambiente.pt/). Therefore, validation of sediment transport and soil erosion studies with models must be based on geo-spatial tools. Taking into account that previous studies demonstrated that *lameiros* act as sedimentation-prone areas, we evaluated the role played by this feature in the control of sediment connectivity increase due to fires, by means of evaluating the change of SDR linked to the fires as a function of the density of *lameiros* per sub-basin area. A DEM of Difference (DoD) approach was additionally attempted using two LiDAR-derived DEMs from the PNOA programme (2010 and 2021 coverages, source: IGN Centro de Descargas). However, local differences of up to +24 and − 39 m between the two LiDAR coverages indicated that methodological differences between acquisitions dominate over any real geomorphic signal, rendering this approach unviable for validation in this low-erosion landscape.

3. Results and discussion

3.1. Fire occurrence, recurrence, severity and vegetation dynamics

The total area affected by fires over the 24 years amounts to 15.81 km^2, (49.8% of the surface of the two basins), counting each location only once regardless of recurrence (Table 3). Recurrence of fires –two or more times– during this period happened at the north of each basin and the north at the meeting of the basins. The spatial analysis yielded the following results: one fire (13.89 km^2, 43.7% of the study area), two fires (1.65 km^2, 5.2%), three fires (0.24 km^2, 0.7%) and four fires (0.034 km^2, 0.1%) (Fig. 1d). The burned area per scenario and basin is detailed in Table 4.

During the first scenario (Sc1), the fire-affected areas accounted for 1.02 km^2. Regarding the evolution (Δ) of vegetation (Fig. 2), the change between SC2 and SC1 (ΔSC2–1) showed intense human activity

Table 3
Burned area (km^2) per scenario and basin, derived from high-resolution aerial orthophoto mapping (PNOA series).

Scenario	B.08 (km^2)	B.13 (km^2)
Sc1	0.83	0.2
Sc2	3.72	1.44
Sc3	1.43	3.15
Sc4	0.21	1.34
Sc5	0.23	0.79
Sc6	0.81	0.06
Sc7	0.01	0.12
Sc8	0	1.88
Sc9	0.76	0.41
Sc10	0.14	0.39

Note: Values represent the burned area mapped in each scenario, including areas that may have been burned in previous scenarios (recurrent fires).

Table 4
Burn severity classes based on dNBR values (from Key and Benson, 2006) and assigned C-factor values (based on Panagos et al., 2015a).

Severity level	dNBR values	C-RUSLE factor
Unburned	< 0.1	Assigned for each land use
Low severity	0.1–0.26	0.10
Moderate-low	0.27–0.43	0.20
Moderate-high	0.44–0.65	0.35
High severity	> 0.66	0.55

(changes in roads and firebreaks, about 0.31 km^2) as well as the largest loss of vegetation among scenarios (−5.16 km^2), mainly on the Portuguese side. ΔSC3–2 presented a moderate vegetation loss of 0.81 km^2, reflecting continued fire occurrence and land management practices. In ΔSC4–3, ΔSC5–4, ΔSC6–5 and ΔSC7–6 there was a consistent and intense human activity (new roads and firebreaks), and natural vegetation recovery (without seeding or planting) that counted 4.51, 1.54, 1.02 and 0.86 km^2, respectively. ΔSC7–6 showed a loss of vegetation (−0.12 km^2), while ΔSC8–7 showed a greater loss (−1.88 km^2), representing the second largest loss among the scenarios. In ΔSC9–8, it occurred a vegetation loss of 1.17 km^2, while vegetation recovery added 1.88 km^2. Finally, ΔSC10–9 showed a vegetation loss of 0.52 km^2 due to fires, while vegetation recovery added approximately 1.17 km^2. We observed that subsequent fires did not always occur in the same locations, allowing previously burned areas to regenerate.

Over the 24-year period, new paths and firebreaks were made in 7 of the 10 scenarios. These post-fire activities are common in Spain and Portugal, both to remove burnt wood and to facilitate the prevention and extinction of future fires (Pastor et al., 2020; Beighley and Hyde, 2018). In three scenarios, the number of patches with vegetation loss exceeded the number of patches with vegetation gain. As a summary, 16.3 and 15.5 km^2 lost and gained vegetation, respectively. This fact was already described by Peris-Llopis et al. (2024) in Mediterranean forests where recurrence reduced conifers and broadleaves' cover, modifying vegetation structure, with shrub accumulation that amplified the probability of fire recurrence. The loss of mature shrub and forest vegetation entails a severe loss of soil protection against water erosion, much greater than the gain in protection associated with the recovery of vegetation. Indeed, Shakesby (2011) –after analyzing many fires in Mediterranean countries– discussed about the window of disturbance on sediment yield (SY) caused by fires, with a sharp increment of SY just after the fire and a mild decline until the 'background' SY value is recovered, and how recurrent fires modify this dynamic in two ways: I) extending the duration of the window of disturbance of SY over time, and II) increasing the 'background' SY value in the affected area.

Regarding the fires, moderate-low fire severity was the most frequent in Sc1 ($\overline{dNBR} = 0.336$), Sc2 ($\overline{dNBR} = 0.280$) and Sc3 ($\overline{dNBR} = 0.357$), with 4, 14 and 15 separated burnt areas at each scenario. Low fire severity prevailed in Sc4 ($\overline{dNBR} = 0.246$), Sc5 ($\overline{dNBR} = 0.271$) and Sc6 ($\overline{dNBR} = 0.221$), with 17, 16 and 7 burnt areas, respectively. In Sc7, fire severity increased to moderate-low ($\overline{dNBR} = 0.312$) with 8 burnt areas. And then, low fire severity prevailed in Sc8 ($\overline{dNBR} = 0.161$), Sc9 ($\overline{dNBR} = 0.233$) and Sc10 ($\overline{dNBR} = 0.191$), with 15, 10 and 4 burnt areas, respectively. Overall, low severity was more frequent (six scenarios) that moderate-low severity (four scenarios). In the four scenarios with higher severity (Sc1, Sc2, Sc3 and Sc7), which can have significant implications for soil erosion, the average burnt surface was 116.72 ha per scenario and 275.75 ha per polygon (individual burnt area); whereas during the six low-severity scenarios (Sc4, Sc5, Sc6, Sc8, Sc9 and Sc10), the average burnt surface was 10.14 ha per scenario and 26.90 ha per polygon.

The spatial analysis of the physiographic parameters revealed that the occurrence of fires gradually increases with altitude until the intervals between 812 and 865 m (Fig. 3). The average extent of burned areas was highest between 839 and 865 m (301 ha), while severity also increases, peaking in the range between 1027 and 1085 m ($\overline{dNBR} = 0.358$). Recurrence showed the highest values above 977 m, with records of up to 4 fires in elevated areas (from 897 m upwards) where lower air humidity may occur, with greater exposure to the wind, less human interference, and a greater accumulation of combustible material, as well as making it more challenging to fight the fire initially (Novo et al., 2020; Fernández-García and Alonso-González, 2023). Although it does not act in isolation, altitude contributes to the recurrence of fires when associated with elements such as vegetation, topography, and human action, which determine fire behavior in Mediterranean environments (Barbati et al., 2015; Peris-Llopis et al., 2024). Regarding the orientation, there was a greater extent of burning in areas facing southwest (333 ha) and south (242 ha), as well as slightly higher severity and recurrence values between SE and SW. North-facing areas showed a smaller affected area and lower recurrence. This pattern can be explained by the greater solar incidence on the southern and southwestern slopes in the northern hemisphere, which leads to greater evapotranspiration and, consequently, less moisture in the vegetation and soil, making them more susceptible to fire ignition and spread (Shakesby, 2011; Metzen et al., 2019). Orientation also influences the thermo-hydraulic behavior of the soil, with drying rates, higher on slopes more exposed to solar radiation, regardless of vegetation cover (Oorthuis et al., 2020). Areas to the north, with less solar exposure, tend to maintain greater humidity and have a greater capacity for post-fire regeneration (Rodrigues et al., 2024).

Fires occurred predominantly in gentle slopes (0–0.6 m/m), with high severity (dNBR >0.27) in the lower ranges. From 0.6 m/m onwards, both the occurrence, extent, and recurrence decreased. This may be related to the fact that gentle slopes facilitate the spread of fire, while steeper slopes reduce the accumulation of combustible material and make it more difficult for flames to advance (Wang and Zhou, 2023). Vegetation cover, based on the C-factors, also influenced and fires mainly occurred in areas with very low (0–0.1) or very high (0.9–1) C values. Areas with low C, such as scrubland and unmanaged forests, accumulate a large amount of fuel, while high values indicate degraded land with dry material (García-Llamas et al., 2019; Viedma et al., 2020). In addition, previously burned areas are more prone to new fires when recovery is incomplete, or there is recurrence over a short interval, which reduces the resilience of the vegetation and favours the accumulation of fuel(González-De Vega et al., 2016; Fernández-García et al., 2020). The distance of fires from the *lameiros* played a key role in modulating the fire's spread and intensity. There was a tendency for the area burned and the severity of the fires to increase with distance from the *lameiros*. In areas very close to (0–10 m), the frequency and severity of fires were extremely low, with average burnt areas of just 4 ha at a 5 m distance. In contrast, fires became significantly more frequent and severe at further distances (>50 m), reaching an average of 31 ha at 100 m from the *lameiros*. These results reinforce the importance of *lameiros* as a

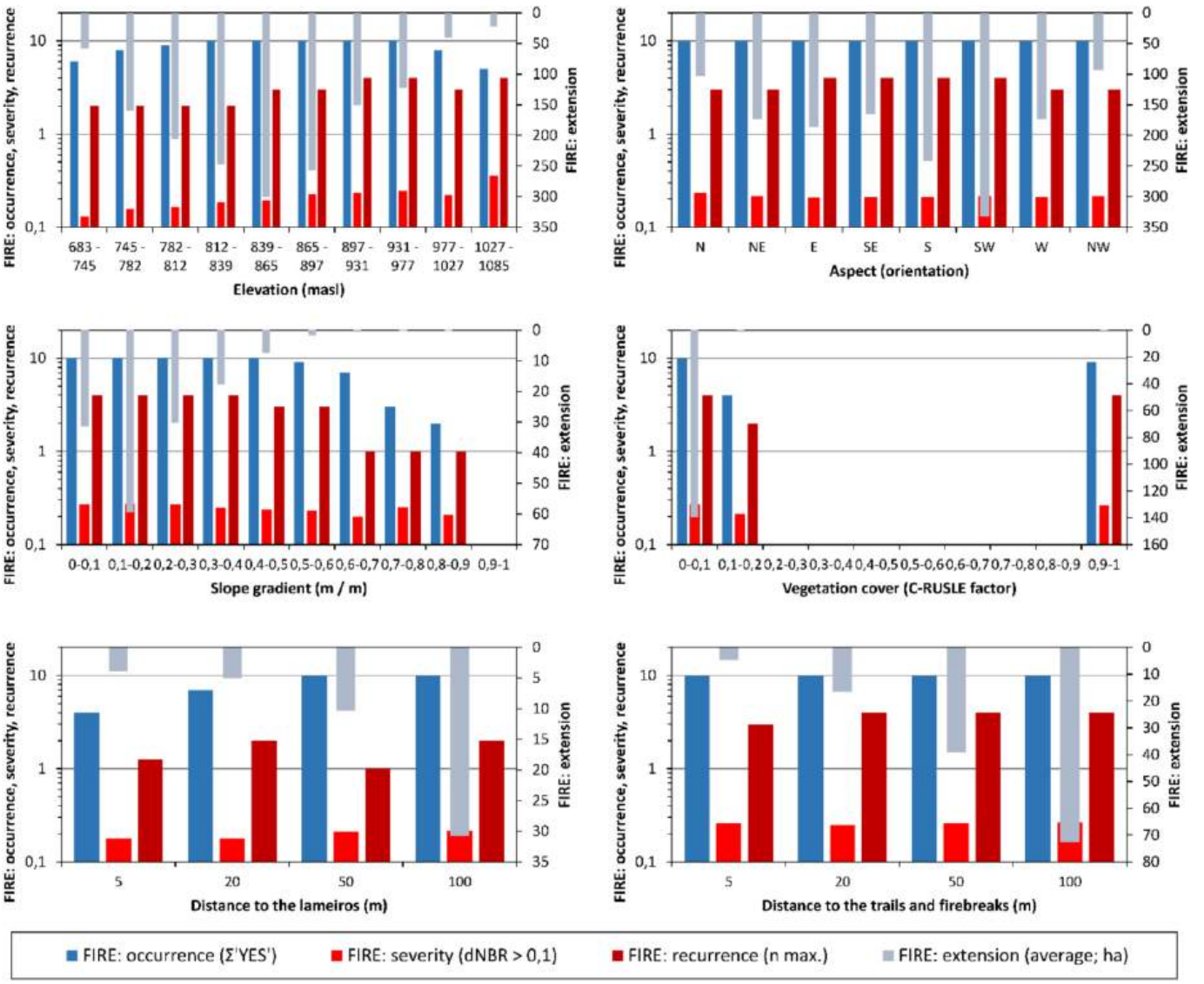

Fig. 3. Relationship between fire and physiographic parameters. These charts were generated considering the average conditions over the ten temporal scenarios analyzed in this study.

landscape element capable of mitigating the effects of fire, acting as natural barrier to its spread.

The recurrence of fires in *lameiros* was generally low, with a maximum of two that was only observed in the class of *lameiros* in use with river, where the area burned represented just 0.0165% of the total area of this class. When considering one fire occurrence, *lameiros* in use without river showed the highest proportion of burned areas at 0.0746% of their total class area, suggesting that the absence of watercourses may increase vulnerability to fire (Turco et al., 2017; Ruffault et al., 2023). Despite this, areas near river concentrated a greater absolute burnt area, possibly due to greater exposure to ignition sources associated with human presence and management. This pattern, observed in regions of Turkey and the Mediterranean arc, highlights the significant role of human activities in fire occurrence (Ganteaume et al., 2013; Elia et al., 2019). The predominance of intentional causes during the 24-year period of study (Supplementary Table 2) also reinforces the role of accessibility as a risk factor.

In abandoned *lameiros*, the absence of watercourses may have contributed to greater fire vulnerability, similar to what was observed in *lameiros* in use without river, along with the additional aggravating factor of abandonment. Abandoned *lameiros* with river had 13.16% of their area burned once, while those without river exhibited more than double this proportion, with 31.60% of their area burned once. Abandonment favours the accumulation of dry biomass, and the lack of water reduces soil and vegetation moisture, facilitating fire spread even in areas with lower vegetation density. Dry fuel significantly increases fire size in Mediterranean areas, and biomass accumulation due to landscape abandonment intensifies fire spread (Loepfe et al., 2010; Bertomeu et al., 2022). In abandoned agricultural contexts, these areas accumulate herbaceous vegetation, becoming more vulnerable to fire spread(Carlos Silva et al., 2019).

Additionally, the frequency of fires did not vary significantly with distance from trails and firebreaks, yet areas close to these features exhibited lower severity and extent of burning. These man-made elements thus played a dual role: on one hand, acting as physical barriers and access routes for firefighting, which facilitated fire control and disrupted vegetation continuity (Wang et al., 2021); on the other hand, their accessibility increased vulnerability to arson-caused wildfires (Costafreda-Aumedes et al., 2017).

The evolution of the ten maps of the C factor reflected the changes in the vegetation cover due to the multiple fires (higher C values), the progressive vegetation recovery (lower C values) and human activities

(new or abandoned unpaved forest trails, firebreaks, and paved mountainous road; higher C values) (Fig. 4). As expected, the lowest C values appeared in the Sc0, before occurrence of fires ($\overline{C}_{B.08}$ = 0,0456; $\overline{C}_{B.13}$ = 0,0543). In the first scenarios (Sc1 and Sc2), C values increased, associated with the greater burnt area, especially in Sc2 (+16.23% accounting the two basins). From Sc3 to Sc6, a stabilization or slight reduction was observed following the start of vegetation recovery, with Sc3 (23.9% of the area with 3–4 years of regeneration) and Sc4 (wider distribution between ranges of 1 to 14 years) standing out. In Sc7 and Sc8, the C values rose again, owing to the influence of the increase in urban areas and linear elements, especially in B.13. In Sc9 and Sc10, the highest C values were observed ($\overline{C}_{B.08}$ = 0.0684 and $\overline{C}_{B.13}$ = 0.1427 in Sc9; and $\overline{C}_{B.08}$ = 0.0679 and $\overline{C}_{B.13}$ = 0.1473 in Sc10), despite the significant presence of vegetation older than 15 years (16.4% and 28.9%, respectively). This behavior suggested that the influence of the new fires, urban growth and linear infrastructure, which acted as very effective areas of sediment transport, outweighed the positive effect of vegetation regeneration. Overall, a reduction in ground protection took place in both basins, indicating higher risk of soil erosion by water.

Previous studies confirmed an increase in the C factor immediately after fires (Santana et al., 2024; Fernández et al., 2025), corroborating our initial results (Sc1, Sc2). However, available studies are limited to specific time windows or isolated factors, comparing only two points in time (Maxwald et al., 2024), assessing short recovery phases (Evangelides and Nobajas, 2020); Madoui et al., 2015), or neglecting anthropogenic activities (Yang et al., 2022), without systematically tracking temporal evolution over multiple disturbance-recovery cycles. Our approach integrates ten temporal scenarios, capturing both post-fire vegetation dynamics and the cumulative impact of human activities at the basin scale.

3.2. Evolution of sediment connectivity (AIC) and delivery ratio (SDR) due to the fire dynamic

Extreme classes of connectivity (AIC < P10 and AIC > P90) displayed localized variations (Fig. 5). High connectivity (P90) areas were identified in steep slopes, headwaters, and high surface runoff. Low-connectivity (P10) zones were primarily located in valley bottoms and low-slope surfaces; coinciding with the *lameiros*. The areas of intermediate connectivity (P40 < AIC < P60), which showed spatial stability, appeared along transitions between landforms and drainage networks, and were the most affected by fires, up to four episodes. These zones are dominated by continuous and shrubby vegetation and lack natural elements or barriers, such as *lameiros*, which can ease the occurrence of fire propagation corridors, linking disturbance regime and sediment connectivity (Oliveira et al., 2021; Peris-Llopis et al., 2024).

Those areas with persistent percentiles over the ten scenarios highlighted the control of structural connectivity over sediment delivery. Persistent P90 AIC areas remained in topographically exposed, sloping areas, and overlapped less with regions of high fire recurrence, indicating a certain degree of soil conservation. This fact may be explained due to the discontinuous vegetation and microclimatic conditions of these areas, being less conducive to ignition (García-Llamas et al., 2020; Viedma et al., 2020).

Persistent P10 AIC zones were found in more stable morphological compartments, such as embedded valleys and deposition zones. This spatial persistence demonstrates that landscape configuration directly controls sediment connectivity, even in man-made modified landscapes. In summary, fire modulates the intensity and spatial distribution of sediment transport, but primarily amplifies susceptibility in already vulnerable areas (González-Romero et al., 2021; Clark et al., 2025). This work is the first to combine continuous sediment connectivity mapping with specific analysis of recurring fire regimes over a decade. It provides a new perspective on sediment transport in Mediterranean landscapes affected by multiple fires.

The spatial patterns of SDR, and the temporal changes among scenarios, mirrored those of AIC (Fig. 6). Scenarios with increased fire activity (Sc2, Sc3 and Sc7) showed marked rises in SDR, particularly where steep slopes coincided with high fire severity. In contrast, the most recent scenarios (Sc9 and Sc10) displayed a more dispersed pattern of high SDR, indicating gradual vegetation recovery. Over time, SDR patterns shifted from concentrated zones of effective sediment delivery after fire events to more fragmented distributions during recovery, reducing sediment transport from sediment sources to channels. In post-fire basins, slope gradient controls sediment delivery by increasing the potential for sediment movement downslope after vegetation loss, due to reduced surface roughness and interception, which favours the formation of more efficient sediment pathways (González-Romero et al., 2021; Follmi et al., 2022). The severity of fires in Sc2, Sc3 and Sc7 was closely linked to persistent corridors of SDR. Research indicates that higher fire severity extends periods of elevated sediment transport in watersheds (Mayor et al., 2007; De Girolamo et al., 2022), with the most affected areas maintaining sediment delivery-prone conditions for longer periods (López-Vicente et al., 2021; Alexiou et al., 2024). Hydrophobic soil layers induced by fire may contribute to this effect by increasing runoff and erosion (Mongil-Manso et al., 2024) and factors such as soil structure, topography, vegetation cover and land management also significantly influence sediment transport in Mediterranean environments (López-Vicente and Ben-Salem, 2019; Llena et al., 2019).

In a first analysis and without considering the dependence of SDR to

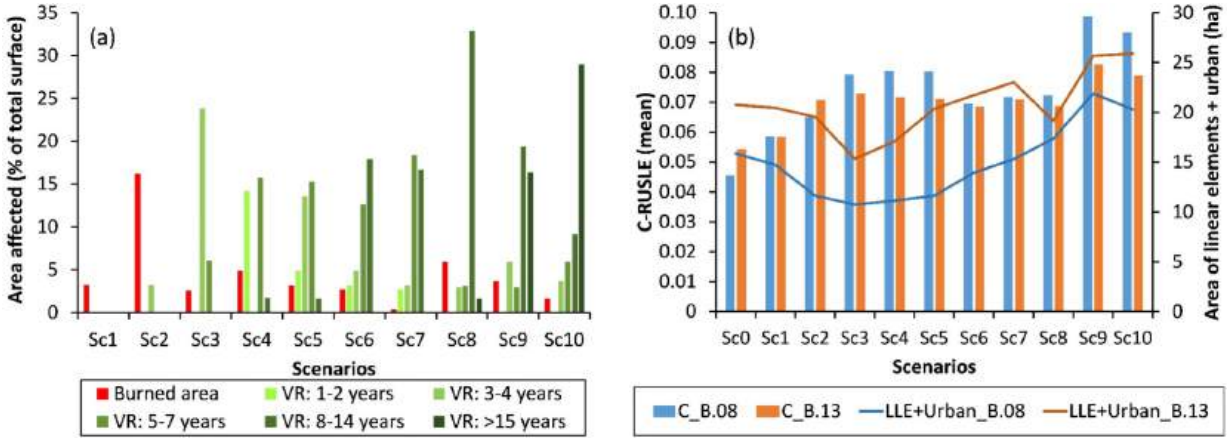

Fig. 4. (a) Percentage of the total area affected by new fires in the two basins, and by vegetation recovery classes (VR: 1–2, 3–4, 5–7, 8–14, >15 years), for each scenario (SC1–SC10). (b) Mean C-RUSLE values per basin, and total area (ha) occupied by the man-made elements (roads, firebreaks, trails and urban area) for each scenario and basin.

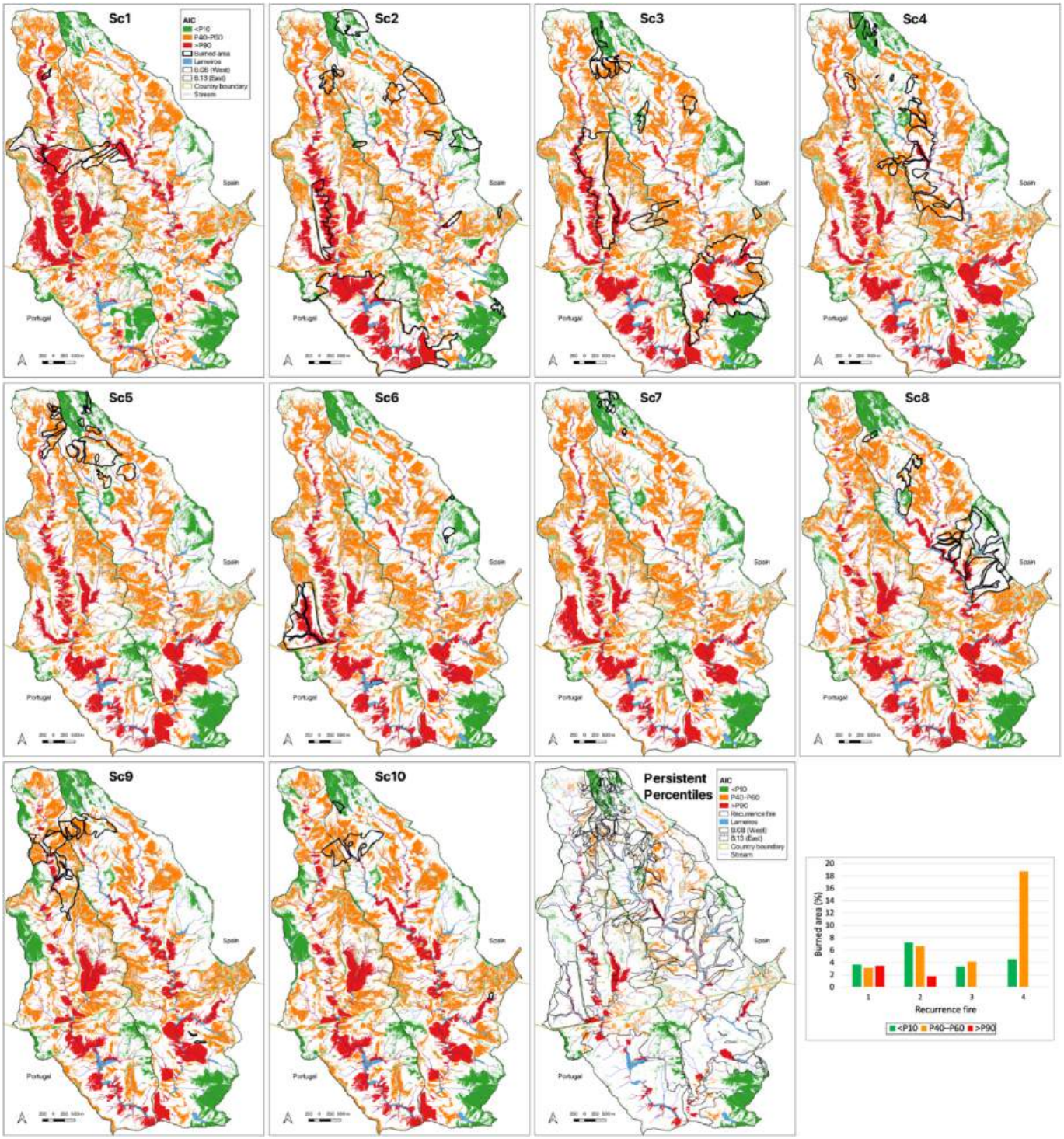

Fig. 5. Evolution over the ten scenarios of the spatial location of the areas of AIC corresponding to the percentiles <P10, between P40 and P60, and > P90. Percentiles were calculated for each basin and scenario independently.

the upslope drainage area, *lameiros* ($\overline{SDR_{Sc01-10\_lameiros}}$ = 0.0404 ± 0.0069 and 0.0238 ± 0.0034 in B.08 and B.13) showed similar SDR values to those obtained at the basin scale ($\overline{SDR_{Sc01-10\_basin}}$ = 0.0345 ± 0.0026 and 0.0248 ± 0.0022 in B.08 and B.13) –in spite of their spatial location in or next to the stream system– and also similar to the SDR in the fire affected areas ($\overline{SDR_{Sc01-10\_burnt}}$ = 0.0360 ± 0.0114 and 0.0238 ± 0.0101 in B.08 and B.13), which are located in the hillslopes and further away to the streams. These values agreed with the complex sedimentological behavior of *lameiros* the act as buffer zones, reducing the transfer of sediment from adjacent slopes (Bertocco et al., 2025). This retention function remained evident throughout the time series, even after episodes of burning in the surrounding areas.

To refine the analysis of the specific role played by fires and *lameiros* in the temporal evolution of SDR, the two basins were divided into 756 small sub-basins (SB), which 393 are located in B.08 and 363 in B.13 (Fig. 7a). Over the 24-year study period, 549 sub-basins contained burnt areas in at least one scenario, while 207 remained unburnt. These SB

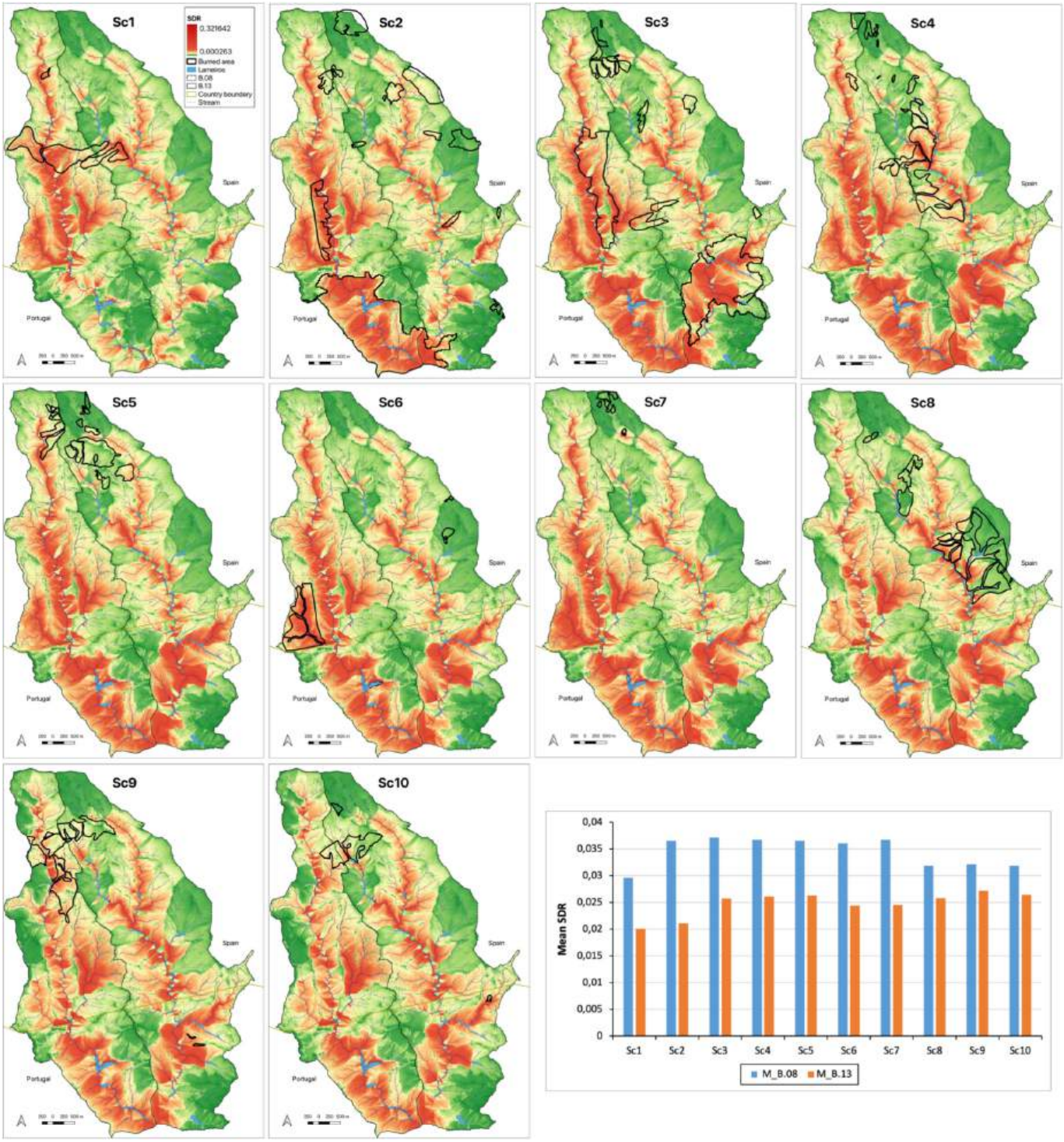

Fig. 6. Maps of SDR calculated for the ten scenarios. The bar graph shows the mean SDR value obtained for each scenario and basin.

were classified into four categories: SB with burnt areas and without *lameiros* (SB-I), SB with burnt areas and with *lameiros* (SB-II), SB without burnt areas and without *lameiros* (SB-III), and SB without burnt areas and with *lameiros* (SB-IV). The number and spatial location of SB with burnt areas changed over the ten scenarios (Supplementary Fig. 1). The effect of the drainage area (***A*** factor in eq. (3)) at each SB was added by means of calculating the ratio SDR/A. The results indicated that *lameiros* played a stabilising role in sediment transport, favouring the resilience of fluvial sub-basins. Among SB affected by fires, SB-I presented higher mean SDR/A values (0.00033) compared to SB-III (0.00021), along with a greater standard deviation, suggesting higher sensitivity to local environmental variations, such as slope, soil properties, and fire intensity (Shakesby & Doerr, 2006; Vieira et al., 2018). The approximately 36% reduction in SDR/A in SB-II confirms the capacity of *lameiros* to mitigate post-fire erosion effects, acting as regulating elements of sediment transfer. In unburnt SB, the reduction made by *lameiros* was only 7%, confirming that their stabilising effect is maintained even in the absence of disturbances, promoting temporary deposition and limiting sediment connectivity between hillslopes and channels (Abebe et al., 2023). These percentages are specific to the AIC configuration used in

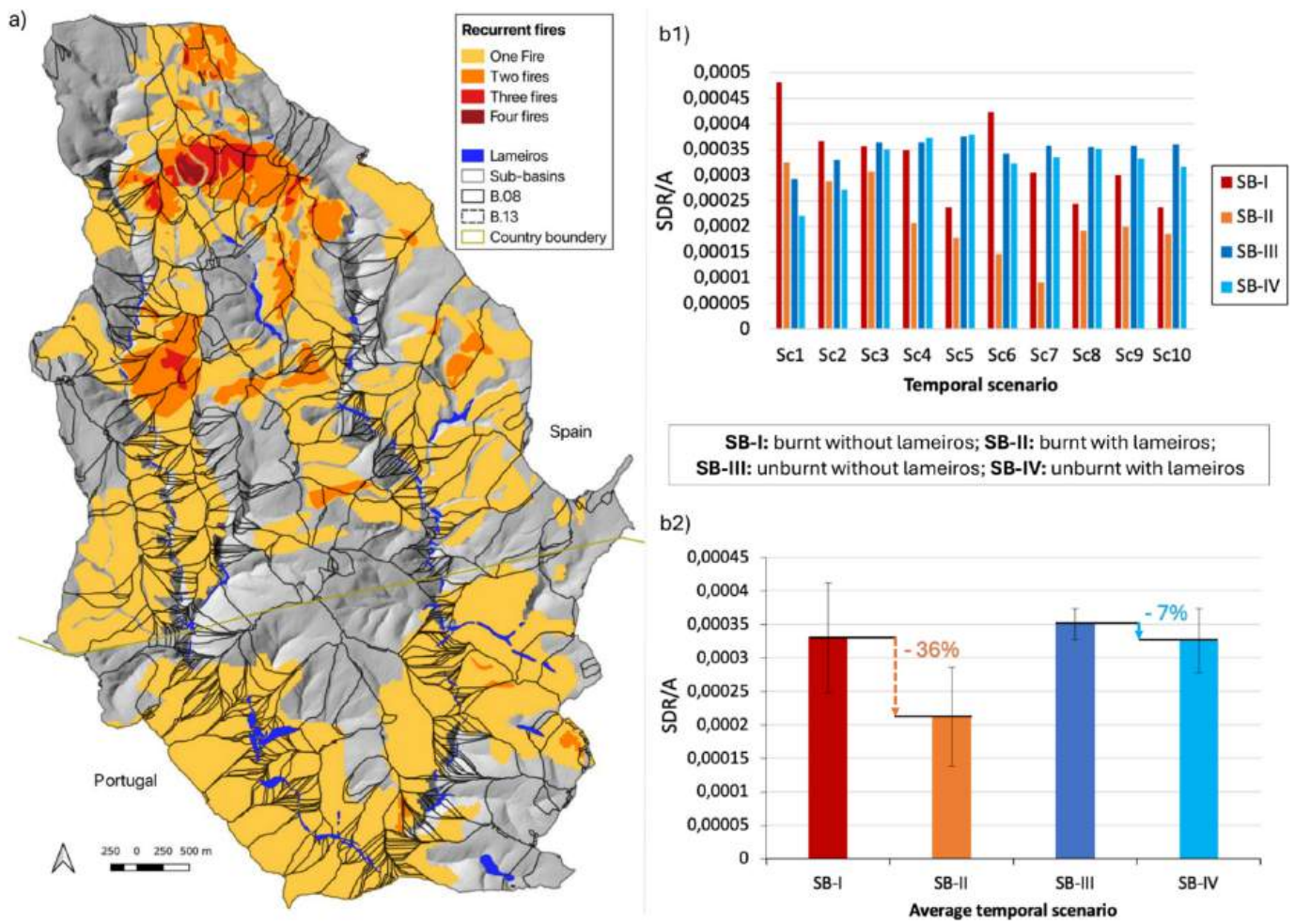

Fig. 7. Map of the 756 sub-basins (SB), and bar plots of the ratio SDR/A in the four types of SB: SB-I, SB-II, SB-III and SB-IV.

this study, where the permanent stream network was chosen as the computational target (see Section 2.5). The spatial proximity of *lameiros* to the stream network means that their buffering effect is maximised in this configuration, particularly in burnt sub-basins where sediment pathways from hillslopes to streams are more direct and **efficient**. Three complementary factors can explain this marked contrast. First, fire removes vegetation cover, drastically increasing SDR/A in sub-basins without *lameiros*, making *lameiros* proportionally much more effective as sediment barriers in post-fire conditions. In unburnt sub-basins, vegetation already provides natural protection, and SDR/A is naturally low, reducing the relative contribution of *lameiros*. Second, *lameiros* are located within or adjacent to the permanent stream network, the computational target of the AIC, meaning their intercepting role is directly captured in the SDR maps. In burnt sub-basins, the absence of vegetation amplifies sediment transfer from hillslopes to streams, further enhancing the measured buffering effect of *lameiros*. Third, despite SB-II having a steeper mean slope than SB-I (19.8% vs 16.9%), it presents lower SDR/A values, demonstrating that *lameiros* can override topographic controls on sediment delivery under post-fire conditions. Additionally, the density of *lameiros* in each SB was estimated (Supplementary Table 6), providing complementary information on their spatial distribution and potential influence on SDR/A variability.

The comparison between SB revealed that the presence of *lameiros* mitigate or even counteract the effect of topographic gradient on sediment transport. SB-II presented a lower SDR/A than SB-I, despite having a steeper slope ($\overline{S}$=19.8% vs. $\overline{S}$=16.9%), a pattern also observed between SB-IV and SB-III ($\overline{S}$=22.8% vs. $\overline{S}$=18.2%). In the absence of *lameiros* (SB-I and SB-III), fires increased the variability of sediment transport potential. However, mean values remained relatively similar between SB-I and SB-III, with contrasting temporal evolution potentially associated with different patterns of vegetation loss and recovery, as well as the spatial location of burnt areas in relation to the hydrographic system. Overall, these results corroborate Bertocco et al. (2025), who, when analyzing *lameiros* over a complete annual cycle, observed a predominance of sedimentation over transfer, especially during wet periods. Whilst that study documented this stability under seasonal variations, the ten scenarios of the present work demonstrate the same regulatory function under different topographic gradients and fire disturbances, confirming that *lameiros* act as sediment disconnectivity zones regardless of the temporal or spatial scale of analysis.

3.3. Role of lameiros in buffering sediment delivery under recurrent fire regimes

The mean rainfall erosivity was 941.28 and 947.05 MJ mm ha^{-1} h^{-1} yr^{-1} in B.08 and B.13; and at the most recent scenario, year 2020, to which the latest actual land cover map dates back, the modelled mean soil erosion was approximately 3.34 and 3.96 Mg ha^{-1} yr^{-1} in B.08 and B.13 (Fig. 8a). The distribution of soil erosion rates showed distinct patterns between the two basins. In the very low erosion class ($E^{-} \leq 1.4$ Mg ha^{-1} yr^{-1}), B.08 had 27.7% of its area, while B.13 recorded only 17.5%. For low erosion ($1.4 < E^{-} \leq 2$ Mg ha^{-1} yr^{-1}), both basins showed low values: 3.6% in B.08 and 4.3% in B.13. In the moderate erosion class ($2 < E^{-} \leq 5$ Mg ha^{-1} yr^{-1}), 17.0% of B.08 and 20.7% of B.13 were affected. High erosion ($5 < E^{-} \leq 11$ Mg ha^{-1} yr^{-1}) was more pronounced

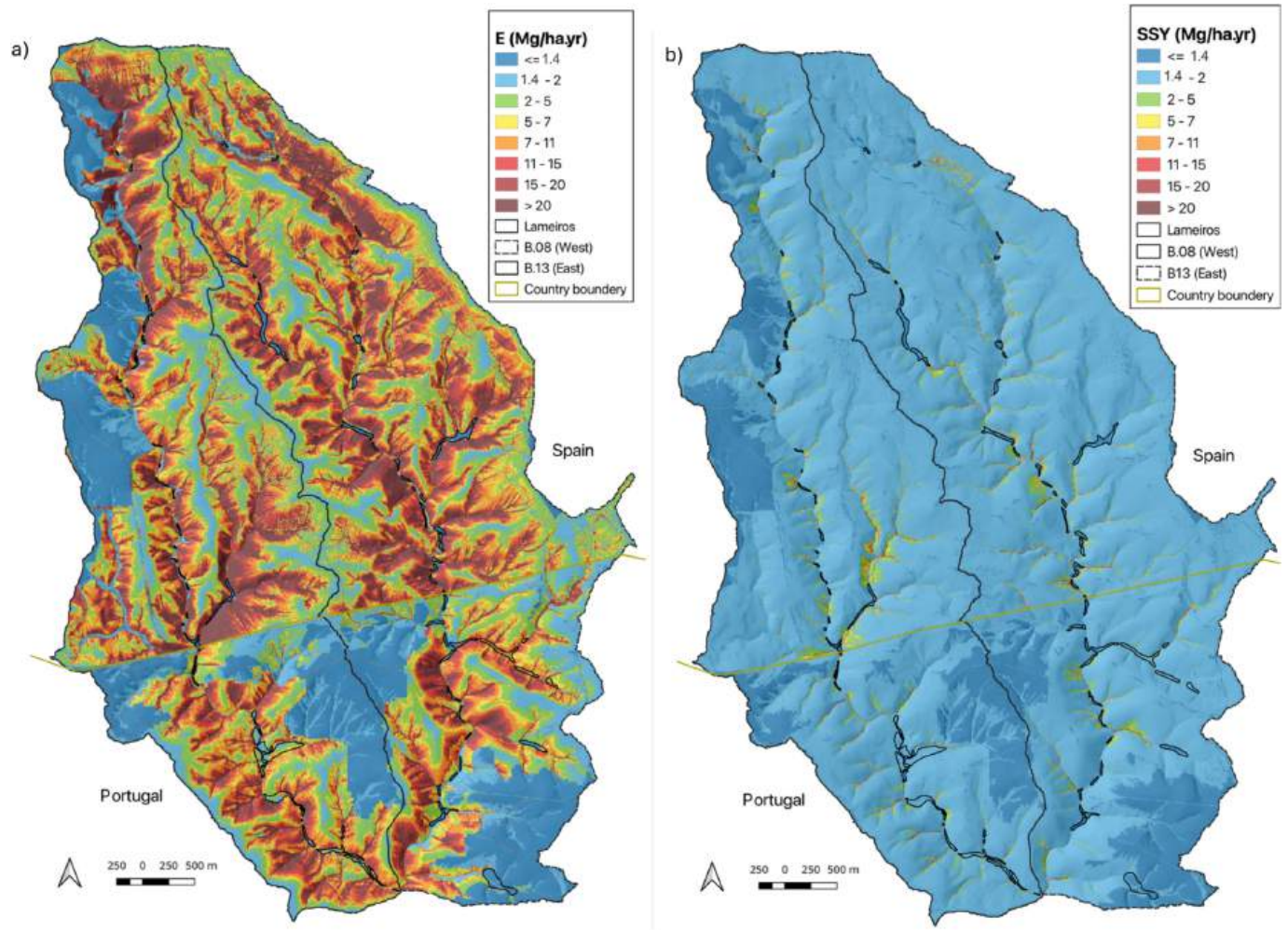

Fig. 8. Maps of soil erosion (a) and sediment yield (b) estimated for the year 2020 in the two basins.

in B.13 (27.5%) compared to B.08 (24.6%). Finally, very high erosion ($E^- > 11$ Mg ha^{-1} yr^{-1}) affected 28.1% of B.08 and 30.1% of B.13. This comparative analysis reveals that B.08 exhibited a polarised distribution, with simultaneous dominance of areas with very low and very high erosion, while the intermediate classes were less represented. In contrast, B.13 showed a distribution more concentrated in the higher classes (high and very high erosion), with lower representation of the lower classes, indicating a landscape with generally higher erosion vulnerability.

The average erosion rates in B.08 and B.13 were slightly above the mean values of 2.46 Mg ha^{-1} yr^{-1} in Europe, 2.31 in Portugal, and 3.94 in Spain (ESDAC, 2020). These differences were associated to the effect of forest fires. According to Panagos et al. (2015), mean erosion rates by land cover type in Europe are: forests (0.07 Mg ha^{-1} yr^{-1}), pastures (2.02), shrub and herbaceous vegetation (2.69), heterogeneous agricultural areas (4.21), natural grasslands (4.41), and sparsely vegetated areas (40.16).

The contrasting land cover composition between the basins explained the differences observed in the distribution of erosion classes. In B.08, the dominant covers are transitional shrubland (30.8%) and heaths and moors (33.8%), with sparsely vegetated areas representing only 3.6% and natural grasslands 3.0%. Sparsely vegetated areas are concentrated in specific locations (usually rocky outcrops or degraded zones), creating hotspots of very high erosion (40.16 Mg ha^{-1} yr^{-1}), explaining the polarised distribution characteristic of this basin.

By contrast, B.13 is dominated by heaths and moors (54.0%), followed by natural grasslands (13.3%), sparsely vegetated areas (9.2%), and transitional shrubland (only 8.0%). This configuration results in a landscape more uniformly vulnerable to erosion: the extensive cover of heaths and moors, combined with the higher proportion of natural grasslands (4.41 Mg ha^{-1} yr^{-1}) and sparsely vegetated areas, explains the concentration of areas in the high and very high erosion classes.

Lameiros, although occupying only 1.1% of the area in B.08 ($E^- =$ 5.19 Mg ha^{-1} yr^{-1}) and 1.2% in B.13 ($E^- = 10.0$ Mg ha^{-1} yr^{-1}), play a strategic role in erosion mitigation because of their hydrological connectivity. Differentiated hydrological connectivity with adjacent coverings of contrasting erosion also contributes (Fryirs, 2013; Baartman et al., 2013). Although the processes of soil erosion also affected *lameiros*, their strategic position and (dis)connectivity have a disproportionate effect on geomorphological stability. *Lameiros* act as buffer zones that intercept and retain sediments from adjacent, more vulnerable areas. Their role is especially critical in B.13, where the greater extent of vulnerable covers amplifies sediment production. In both basins, this role is even more important after recent disturbances such as wildfires. Burnt areas can cause abrupt increases in soil loss, especially on steep and unprotected slopes (Noske et al., 2024).

The total sediment yield (SY) estimated with RUSLE-AIC-SDR was 321.9 and 343.6 Mg yr^{-1} in B.08 and B.13, with mean area-specific sediment yields (SSY) of 0.227 and 0.205 Mg ha^{-1} yr^{-1}, respectively (Fig. 8b). These relatively low basin-scale SSY are noteworthy when compared with the typical post-fire behavior observed in other Mediterranean regions. For instance, Mastrolonardo et al. (2024) reported abrupt increases in sediment delivery in southern Italy during the years immediately following fire events, largely driven by enhanced hydro-

sedimentary connectivity under post-disturbance conditions. Such increases are controlled by multiple interacting factors that vary temporally during recovery periods of about two years, including vegetation regrowth, rainfall intensity, and soil surface conditions (Nunes et al., 2021). The absence of comparable sediment peaks in our study basins, despite recurrent fire occurrence, highlights their remarkable resilience. This resilience can be attributed to the structural disconnectivity provided by valley-bottom *lameiros* and the local physiographic configuration, which effectively interrupt sediment transfer pathways and promote local sediment storage. These patterns are consistent with the sediment connectivity framework reviewed by Shi et al. (2025), in which landscape elements that disrupt both structural and functional connectivity act as effective barriers to sediment transfer, maintaining basin stability even under recurrent disturbance conditions.

3.4. Current soil erosion and sediment yield and model validation

Due to the lack of gauging stations in the two basins of this study, a qualitative validation of the results of SSY estimates was done based on field observations (Supplementary Fig. 2). Our results were consistent with the absence of visible rills, ephemeral gullies, slope failures, landslides, or erosional scars in valley bottoms. The physiography of our study area is unique: minimal agricultural area, along with very little livestock activity, and the presence of *lameiros*, strategically located in valley bottoms along rivers and main watercourses. These conditions occur in very few regions of Spain, Portugal and other countries, limiting direct comparisons. Our results are consistent with the low soil loss values reported in nearby regions of Galicia (NW Spain; Mirás-Avalos et al., 2009) and northern Portugal (de Figueiredo et al., 2012) with comparable physiography and land use, supporting the reliability of the model outputs. Regarding the limitations of this study, the SDR calibration parameters were set to default literature values due to the absence of gauging stations, which may introduce uncertainty in the absolute SSY estimates, though not in the relative temporal comparisons. The rainfall erosivity factor (R) was treated as a structural variable with no temporal variation, which may underestimate actual sediment yield during years with extreme rainfall events. Finally, the study focuses on two relatively small transboundary headwater basins with a specific physiographic context, which should be considered when extrapolating results to other landscapes.

3.5. Soil conservation recommendations

Based on these results, soil conservation in these and similar Mediterranean mountain basins should prioritize the active maintenance of *lameiros* currently in use and the restoration of those abandoned, particularly in B.13, where erosion vulnerability is higher, following the approach initiated by the HabMonte project (ICNF, 2020). Active practices of preservation and restoration of *lameiros* can be framed as nature-based, cost-effective solutions (International Union for Conservation of Nature – *IUCN*, 2020), since restoring natural hydrological regimes in fire-prone landscapes has been identified as an effective approach to increase ecosystem resilience (Muñoz-Rojas et al., 2023; Lecina-Diaz et al., 2023). Restoration efforts should focus especially on *lameiros* located within 20 m of the stream network, as these show the strongest buffering effect on SDR. Additionally, the construction of new linear infrastructure near *lameiros* should be minimised, as such infrastructure increases sediment connectivity.

4. Conclusions

This study demonstrates that *lameiros* are crucial components for maintaining hydrosedimentary stability in headwater basins affected by recurrent fires. The results' spatial analysis of ten temporal scenarios, covering 24 years and multiple forest fires, proves that *lameiros* clearly reduce fire severity and recurrence, consistently acting as natural barriers to the spread of flames. *Lameiros* also effectively disconnect sediment flow. Sub-basins with *lameiros* maintain lower sediment delivery ratios, even during severe disturbance or challenging topography (steep slopes). This stabilising effect remains present in all scenarios, reducing post-fire variability and limiting sediment transfer to the drainage network. In contrast, areas without *lameiros* were more connected and experienced higher, more intense peaks of sediment delivery. Current soil erosion and sediment yields in the two paired basins with *lameiros* stay low despite recurrent disturbance, emphasizing the protective role of *lameiros*. To strengthen the resilience of Mediterranean mountain landscapes as fire pressure increases under climate change scenarios, it is essential for stakeholders, policymakers, and land managers to prioritize active practices of preservation, maintenance and restoration of *lameiros*, particularly those currently abandoned, as nature-based, cost-effective solutions, that support targeted conservation actions and effective management strategies. Despite the inherent limitations of modelling sediment transport in ungauged basins, the consistent application of the RUSL*E*-AIC-SDR framework across all ten scenarios ensures robust spatiotemporal comparisons, and field observations and regional literature support the results. Further research with drones will include monitoring of high resolution changes of topography in those areas expected to suffer net soil loss or deposition.

CRediT authorship contribution statement

T. Bertocco: Writing – review & editing, Visualization, Validation, Software, Investigation, Formal analysis, Data curation, Conceptualization. **S.L. Santarén:** Software. **T. de Figueiredo:** Supervision. **R.F.F. Henriques:** Supervision. **M. López-Vicente:** Writing – review & editing, Writing – original draft, Visualization, Validation, Supervision, Software, Resources, Project administration, Methodology, Investigation, Funding acquisition, Formal analysis, Data curation, Conceptualization.

Declaration of competing interest

The authors declare that they have no known competing financial interests or personal relationships that could have appeared to influence the work reported in this paper.

Acknowledgements

Tamires Bertocco was beneficiary of the grants: “Short Term Scientific Mission (STSM) of the COST Action ‘FIRElinks’ (E-COST-GRANT-CA18135-2c2072f3)” of the European Commission, and ‘Individual research grant 2023.02591.BD’ of the Portuguese Foundation for Science and Technology (FCT).

Appendix A. Supplementary data

Supplementary data to this article can be found online at https://doi.org/10.1016/j.catena.2026.110234.

Data availability

Shapefiles used for spatial analysis (Original data) (Local upload in the journal submission system)

References

Abebe, N., Eekhout, J., Vermeulen, B., Boix-Fayos, C., de Vente, J., Grum, B., Hoitink, T., Baartman, J., 2023. The potential and challenges of the ‘RUSLE-IC-SDR’ approach to identify sediment dynamics in a Mediterranean catchment. Catena 233, 107480.
Afonso, N., Arrobas, M., 2009. Contribuição para a Elaboração da Carta de Solos da Cidade de Bragança. Qualidade do Ambiente Urbano. Novos Desafios 137–142.
Agbeshie, A.A., Abugre, S., Atta-Darkwa, T., Awuah, R., 2022. A review of the effects of forest fire on soil properties. J. For. Res. 33 (5), 1419–1441.

Alexiou, S., Papanikolaou, I., Schneiderwind, S., Kehrle, V., Reicherter, K., 2024. Monitoring and quantifying soil erosion and sedimentation rates in centimeter accuracy using UAV-photogrammetry, GNSS, and t-LiDAR in a post-fire setting. Remote Sens. 16 (5), 802. https://doi.org/10.3390/rs16050802.

Amani, M., Ghorbanian, A., Ahmadi, S.A., Kakooei, M., Moghimi, A., Mirmazloumi, S.M., Brisco, B., 2020. Google Earth Engine cloud computing platform for remote sensing big data applications: a comprehensive review. IEEE J. Sel. Top. Appl. Earth Obs. Remote Sens. 13, 5326–5350.

Baartman, J.E., Masselink, R., Keesstra, S.D., Temme, A.J., 2013. Linking landscape morphological complexity and sediment connectivity. Earth Surf. Process. Landf. 38 (12), 1457–1471.

Barbati, A., Corona, P., D'amato, E., Cartisano, R., 2015. Is landscape a driver of short-term wildfire recurrence? Landsc. Res. 40 (1), 99–108.

Beighley, M., Hyde, A.C., 2018. Portugal Wildfire Management in a New Era Assessing Fire Risks, Resources and Reforms. Centro de Estudos Florestais–Instituto Superior de Agronomia/Universidade de Lisboa.

Bertocco, T., 2021. Caudais de ponta de cheia em bacias de drenagem de lameiros do Parque Natural de Montesinho: estimativas pelo método soil conservation service (SCS) sob cenários de mudança global. Master's final project. Polytechnic Institute of Bragança (IPB), Higher Agrarian School. http://hdl.handle.net/10198/23483.

Bertocco, T., de Figueiredo, T., Paz-González, A., García-Tomillo, A., López-Vicente, M., 2025. Deciphering sediment connectivity dynamic in traditional water-meadows (*lameiros*). Geomorphology 480, 109750. https://doi.org/10.1016/j.geomorph.2025.109750.

Bertomeu, M., Pineda, J., Pulido, F., 2022. Managing wildfire risk in mosaic landscapes: a case study of the upper Gata River catchment in Sierra de Gata, Spain. Land 11 (4), 465.

Carlos Silva, M., do Carmo Bica, M., Soares, P., 2019. From the abandonment of small agriculture to the drama of rural fires. J. Hist. Archaeol. Anthropol. Sci. 4 (1), 1–6.

Cavalli, M., Trevisani, S., Comiti, F., Marchi, L., 2013. Geomorphometric assessment of spatial sediment connectivity in small Alpine catchments. Geomorphology 188, 31–41.

Clark, G.D., Murphy, S.F., Skalak, K., Clow, D.W., Akie, G., Carpenter, K.D., Ebel, B.A., 2025. Hysteretic response of suspended-sediment in wildfire affected watersheds of the Pacific northwest and southern Rocky Mountains. Earth Surf. Process. Landf. 50 (1), e6067. https://doi.org/10.1002/esp.6067.

Colombaroli, D., Gavin, D.G., 2010. Highly episodic fire and erosion regime over the past 2,000 y in the Siskiyou Mountains, Oregon. Proc. Natl. Acad. Sci. USA 107 (44), 18909–18914. https://doi.org/10.1073/pnas.100769210.

Costafreda-Aumedes, S., Comas, C., Vega-Garcia, C., 2017. Human-caused fire occurrence modelling in perspective: a review. Int. J. Wildland Fire 26 (12), 983–998.

de Figueiredo, T., 2013. Uma panorâmica sobre os recursos pedológicos do Nordeste Transmontano. Escola Superior Agrária. (Série Estudos; 84), Bragança. ISBN 978-972-745-138-8. http://hdl.handle.net/10198/8527.

de Figueiredo, T., Fonseca, F., Martins, A., 2012. Soil loss and run-off in young forest stands as affected by site preparation technique: a study in NE Portugal. Eur. J. For. Res. 131 (6), 1747–1760. https://doi.org/10.1007/s10342-011-0581-6.

De Girolamo, A.M., Cerdan, O., Grangeon, T., Ricci, G.F., Vandromme, R., Porto, A.L., 2022. Modelling effects of forest fire and post-fire management in a catchment prone to erosion: impacts on sediment yield. Catena 212, 106080. https://doi.org/10.1016/j.catena.2022.106080.

Desmet, P., Govers, G., 1996. A GIS procedure for automatically calculating the ULSE LS factor on topographically complex landscape units. J. Soil Water Conserv. 51, 427–433.

Editorial, Nature Climate Change, 2017. Spreading like wildfire. Nat. Clim. Chang. 7 (11), 755. https://doi.org/10.1038/nclimate3432.

Elia, M., Giannico, V., Lafortezza, R., Sanesi, G., 2019. Modeling fire ignition patterns in Mediterranean urban interfaces. Stoch. Env. Res. Risk A. 33, 169–181.

Ellett, N.G., Pierce, J.L., Glenn, N.F., 2019. Partitioned by process: measuring post-fire debris-flow and rill erosion with structure from motion photogrammetry. Earth Surf. Process. Landf. 44 (15), 3128–3146.

Evangelides, C., Nobajas, A., 2020. Red-edge normalised difference vegetation index ($NDVI_{705}$) from Sentinel-2 imagery to assess post-fire regeneration. Remote Sens. Appl.: Soc. Environ. 17, 100283.

Fernández, C., Fernández-Alonso, J.M., Vega, J.A., 2020. Exploring the effect of hydrological connectivity and soil burn severity on sediment yield after wildfire and mulching. Land Degrad. Dev. 31 (13), 1611–1621.

Fernández, G., Merchán, L., Sánchez, J.Á., 2025. Spatial representation of soil Erosion and vegetation affected by a Forest fire in the sierra de Francia (Spain) using RUSLE and NDVI. Land 14 (4), 793.

Fernández-García, V., Alonso-González, E., 2023. Global patterns and dynamics of burned area and burn severity. Remote Sens. 15 (13), 3401.

Fernández-García, V., Marcos, E., Fule, P.Z., Reyes, O., Santana, V.M., Calvo, L., 2020. Fire regimes shape diversity and traits of vegetation under different climatic conditions. Sci. Total Environ. 716, 137137.

Fernandez-Manso, A., Quintano, C., Roberts, D.A., 2016. Burn severity influence on post-fire vegetation cover resilience from Landsat MESMA fraction images time series in Mediterranean forest ecosystems. Remote Sens. Environ. 184, 112–123.

Follmi, D., Baartman, J., Benali, A., Nunes, J.P., 2022. How do large wildfires impact sediment redistribution over multiple decades? Earth Surf. Process. Landf. 47 (13), 3033–3050.

Fryirs, K., 2013. (dis) connectivity in catchment sediment cascades: a fresh look at the sediment delivery problem. Earth Surf. Process. Landf. 38 (1), 30–46.

Ganteaume, A., Camia, A., Jappiot, M., San-Miguel-Ayanz, J., Long-Fournel, M., Lampin, C., 2013. A review of the main driving factors of forest fire ignition over Europe. Environ. Manag. 51, 651–662.

García-Llamas, P., Suárez-Seoane, S., Taboada, A., Fernández-Manso, A., Quintano, C., Fernández-García, V., Calvo, L., 2019. Environmental drivers of fire severity in extreme fire events that affect Mediterranean pine forest ecosystems. For. Ecol. Manag. 433, 24–32.

García-Llamas, P., Suárez-Seoane, S., Fernández-Manso, A., Quintano, C., Calvo, L., 2020. Evaluation of fire severity in fire prone-ecosystems of Spain under two different environmental conditions. J. Environ. Manag. 271, 110706.

González-De Vega, S., De las Heras, J., Moya, D., 2016. Resilience of Mediterranean terrestrial ecosystems and fire severity in semiarid areas: responses of Aleppo pine forests in the short, mid and long term. Sci. Total Environ. 573, 1171–1177.

González-Romero, J., López-Vicente, M., Gómez-Sánchez, E., Peña-Molina, E., Galletero, P., Plaza-Alvarez, P., Lucas-Borja, M.E., 2021. Post-fire management effects on sediment (dis) connectivity in Mediterranean forest ecosystems: channel and catchment response. Earth Surf. Process. Landf. 46 (13), 2710–2727.

Guo, Z., Yan, Z., PaErHaTi, M., He, R., Yang, H., Wang, R., Ci, H., 2023. Assessment of soil erosion and its driving factors in the Huaihe region using the InVEST-SDR model. Geocarto Int. 38 (1), 2213208.

Halecki, W., Kruk, E., Ryczek, M., 2018. Evaluation of water erosion at a mountain catchment in Poland using the G2 model. Catena 164, 116–124. : https://doi.org/10.1016/j.catena.2018.01.014.

Hamel, P., Chaplin-Kramer, R., Sim, S., Mueller, C., 2015. A new approach to modeling the sediment retention service (InVEST 3.0): case study of the cape fear catchment, North Carolina, USA. Sci. Total Environ. 524, 166–177.

Häusler, M., Nunes, J.P., Soares, P., Sánchez, J.M., Silva, J.M., Warneke, T., Pereira, J.M., 2018. Assessment of the indirect impact of wildfire (severity) on actual evapotranspiration in eucalyptus forest based on the surface energy balance estimated from remote-sensing techniques. Int. J. Remote Sens. 39 (20), 6499–6524.

ESDAC – European Soil Data Centre, 2020. Soil Loss by Water erosion in Europe. Access. https://esdac.jrc.ec.europa.eu/themes/rusle2015.

ICNF, 2020. HabMonte - Projeto de Prevenção Estrutural e Conservação de Habitats Naturais Protegidos e Espécies Prioritárias do Parque Natural de Montesinho. Instituto da Conservação da Natureza e das Florestas, Lisboa, Portugal.

IUCN (Ed.), 2020. IUCN Global Standard for Nature-Based Solutions, First edition. IUCN, Gland, Switzerland. https://doi.org/10.2305/IUCN.CH.2020.08.en.

Jin, X., Liu, Y., Yu, X., 2024. Connectivity-mediated SOC and soil texture variation in the planted shrub ecosystem in the Loess Plateau, China. Catena 239, 107967. https://doi.org/10.1016/j.catena.2024.107967.

Key, C.H., Benson, N.C., 2006. Landscape assessment (LA). In: FIREMON: Fire effects monitoring and inventory system, 164. LA-1.

Lecina-Diaz, J., Campos, J.C., Pais, S., et al., 2023. Stakeholder perceptions of wildfire management strategies as nature-based solutions in two Iberian biosphere reserves. Ecol. Soc. 28 (1), 39. https://doi.org/10.5751/ES-13907-280139.

Liu, L.M., 1994. Calculation model of the sediment delivery ratio on sloping land in gullied rolling loess region. Soil and Water Conservation in China 3 (144), 12–15.

Llena, M., Vericat, D., Cavalli, M., Crema, S., Smith, M.W., 2019. The effects of land use and topographic changes on sediment connectivity in mountain catchments. Sci. Total Environ. 660, 899–912. https://doi.org/10.1016/j.scitotenv.2018.12.479.

Loepfe, L., Martinez-Vilalta, J., Oliveres, J., Piñol, J., Lloret, F., 2010. Feedbacks between fuel reduction and landscape homogenisation determine fire regimes in three Mediterranean areas. For. Ecol. Manag. 259 (12), 2366–2374.

Long, T., Zhang, Z., He, G., Jiao, W., Tang, C., Wu, B., Yin, R., 2019. 30 m resolution global annual burned area mapping based on Landsat images and Google earth engine. Remote Sens. 11 (5), 489.

López-Vicente, M., Ben-Salem, N., 2019. Computing structural and functional flow and sediment connectivity with a new aggregated index: a case study in a large Mediterranean catchment. Sci. Total Environ. 651, 179–191.

López-Vicente, M., Lana-Renault, N., García-Ruiz, J.M., Navas, A., 2011. Assessing the potential effect of different land cover management practices on sediment yield from an abandoned farmland catchment in the Spanish Pyrenees. J. Soils Sediments 11, 1440–1455.

López-Vicente, M., Quijano, L., Palazón, L., Gaspar, L., Navas, A., 2015. Assessment of soil redistribution at catchment scale by coupling a soil erosion model and a sediment connectivity index (central Spanish pre-Pyrenees). Geographical Research Letters 41 (1), 127–147.

López-Vicente, M., González-Romero, J., Lucas-Borja, M.E., 2020. Forest fire effects on sediment connectivity in headwater sub-catchments: evaluation of indices performance. Sci. Total Environ. 732, 139206.

López-Vicente, M., Cerdà, A., Kramer, H., Keesstra, S., 2021. Post-fire practices benefits on vegetation recovery and soil conservation in a Mediterranean area. Land Use Policy 111, 105776. https://doi.org/10.1016/j.landusepol.2021.105776.

Lu, H., Moran, C.J., Prosser, I.P., 2006. Modelling sediment delivery ratio over the Murray Darling basin. Environ. Model Softw. 21 (9), 1297–1308. https://doi.org/10.1016/j.envsoft.2005.04.021.

Madoui, A., Gauthier, S., Leduc, A., Bergeron, Y., Valeria, O., 2015. Monitoring forest recovery following wildfire and harvest in boreal forests using satellite imagery. Forests 6 (11), 4105–4134.

Marques, S.M., Campos, F.S., David, J., Cabral, P., 2021. Modelling sediment retention services and soil erosion changes in Portugal: a spatio-temporal approach. ISPRS Int. J. Geo-Information 10 (4), 262.

Martínez-Murillo, J.F., López-Vicente, M., 2018. Effect of salvage logging and check dams on simulated hydrological connectivity in a burned area. Land Degrad. Dev. 29 (3), 701–712.

Martini, L., Faes, L., Picco, L., Iroumé, A., Lingua, E., Garbarino, M., Cavalli, M., 2020. Assessing the effect of fire severity on sediment connectivity in Central Chile. Sci. Total Environ. 728, 139006.
Mastrolonardo, G., Castelli, G., Certini, G., Maxwald, M., Trucchi, P., Foderi, C., Preti, F., 2024. Post-fire erosion and sediment yield in a Mediterranean forest catchment in Italy. Int. J. Sediment Res. 39, 464–477. https://doi.org/10.1016/j.ijsrc.2024.03.008.
Maxwald, M., Correa, R., Japón, E., Preti, F., Rauch, H.P., Immitzer, M., 2024. Soil and water bioengineering in fire-prone lands: detecting erosive areas using RUSLE and remote sensing methods. Fire 7 (9), 319.
Mayor, A.G., Bautista, S., Llovet, J., Bellot, J., 2007. Post-fire hydrological and erosional responses of a Mediterranean landscpe: seven years of catchment-scale dynamics. Catena 71 (1). https://doi.org/10.1016/j.catena.2006.10.006, 68–7.
Metzen, D., Sheridan, G.J., Benyon, R.G., Bolstad, P.V., Griebel, A., Lane, P.N., 2019. Spatio-temporal transpiration patterns reflect vegetation structure in complex upland terrain. Sci. Total Environ. 694, 133551.
Miller, J.D., Thode, A.E., 2007. Quantifying burn severity in a heterogeneous landscape with a relative version of the delta normalized burn ratio (dNBR). Remote Sens. Environ. 109 (1), 66–80.
Mirás-Avalos, J.M., Paz-González, A., Dafonte-Dafonte, J., Vidal-Vázquez, E., Valcárcel-Armesto, M., 2009. Concentrated flow erosion as a main source of sediments in Galicia, Spain. Earth Surf. Process. Landf. 34 (15), 2087–2095.
Mongil-Manso, J., Ruiz-Pérez, V., López-Sánchez, A., 2024. Infiltration and hydrophobicity in burnt Forest soils on Mediterranean Mountains. Forests 15 (11), 2033. https://doi.org/10.3390/f15112033.
Muñoz-Rojas, M., et al., 2023. Restoring fire-affected soils: the potential of nature-based solutions. J. Environ. Manag. 344, 118544. https://doi.org/10.1016/j.jenvman.2023.118544.
Neary, D.G., Ryan, K.C., DeBano, L.F., 2005. Wildland fire in ecosystems: effects of fire on soils and water. Gen. Tech. Rep. RMRS-GTR-42-vol. 4, 250. US Department of Agriculture, Forest Service, Rocky Mountain Research Station, Ogden, UT, p. 42.
Noske, P.J., Nyman, P., Lane, P.N., Rengers, F.K., Sheridan, G.J., 2024. Changes in soil erosion caused by wildfire: a conceptual biogeographic model. Geomorphology 459, 109272. https://doi.org/10.1016/j.geomorph.2024.109272.
Novo, A., Fariñas-Álvarez, N., Martínez-Sánchez, J., González-Jorge, H., Fernández-Alonso, J.M., Lorenzo, H., 2020. Mapping forest fire risk-a case study in Galicia (Spain). Remote Sens. 12 (22), 3705.
Nunes, J.P., Malvar, M.C., MacDonald, L.H., Ferreira, C.S.S., Martins, M.A.S., Lucas-Borja, M.E., Benavides-Solorio, J., 2021. Key factors controlling the sediment yield in newly-burnt forests: 2-year measurements and modelling. Sci. Total Environ. 753, 141835.
Oliveira, S., Gonçalves, A., Zêzere, J.L., 2021. Reassessing wildfire susceptibility and hazard for mainland Portugal. Sci. Total Environ. 762, 143121. https://doi.org/10.1016/j.scitotenv.2020.143121.
Oorthuis, R., Vaunat, J., Hürlimann, M., Lloret, A., Moya, J., Puig-Polo, C., Fraccica, A., 2020. Slope orientation and vegetation effects on soil thermo-hydraulic behavior. an experimental study. Sustainability 13 (1), 14.
Ougougdal, H.A., Khebiza, M.Y., Messouli, M., Bounoua, L., 2020. Delineation of vulnerable areas to water erosion in a mountain region using SDR-InVEST model: a case study of the Ourika Watershed, Morocco. Sci. Afr. 10, e00646.
Panagos, P., Borrelli, P., Meusburger, K., Alewell, C., Lugato, E., Montanarella, L., 2015a. Estimating the soil erosion cover management factor at the European scale. Land Use Policy 48, 38–50.
Panagos, P., Borrelli, P., Meusburger, K., 2015b. A new European slope length and steepness factor (LS-factor) for modeling soil Erosion by water. Geosciences 5, 117–126.
Panagos, P., Borrelli, P., Meusburger, K., van der Zanden, E.H., Poesen, J., Alewell, C., 2015c. Modelling the effect of support practices (P-factor) on the reduction of soil erosion by water at European scale. Environ Sci Policy 51, 23–34. https://doi.org/10.1016/j.envsci.2015.03.012.
Pastor, E., Muñoz, J.A., Caballero, D., Àgueda, A., Dalmau, F., Planas, E., 2020. Wildland–urban interface fires in Spain: summary of the policy framework and recommendations for improvement. Fire. Technol 56 (5), 1831–1851.
Pausas, J.G., Vallejo, V.R., 1999. The role of fire in European Mediterranean ecosystems. In: Remote Sensing of Large Wildfires: In the European Mediterranean Basin. Springer Berlin Heidelberg, Berlin, Heidelberg, pp. 3–16.
Peris-Llopis, M., Vastaranta, M., Saarinen, N., González-Olabarria, J.R., García-Gonzalo, J., Mola-Yudego, B., 2024. Post-fire vegetation dynamics and location as main drivers of fire recurrence in Mediterranean forests. For. Ecol. Manag. 568, 122126. https://doi.org/10.1016/j.foreco.2024.122126.
Qiao, X., Li, Z., Lin, J., Wang, H., Zheng, S., Yang, S., 2024. Assessing current and future soil erosion under changing land use based on InVEST and FLUS models in the Yihe River basin, North China. Int. Soil and Water Conservation Res. 12, 298–312.
Rahman, S., Chang, H.-C., Hehir, W., Magill, C., Tomkins, K., 2018. Inter-comparison of fire severity indices from moderate (MODIS) and moderate-to-high spatial resolution (Landsat 8 & Sentinel-2a) satellite sensors. IGARSS 2018–2018. IEEE international geoscience and remote sensing symposium. https://doi.org/10.1109/IGARSS.2018.8518449.
Ranzi, R., Le, T.H., Rulli, M.C., 2012. A RUSLE approach to model suspended sediment load in the Lo River (Vietnam): effects of reservoirs and land use changes. J. Hydrol. 422–423, 17–29. https://doi.org/10.1016/j.jhydrol.2011.12.009.
Räsänen, T.A., Tähtikarhu, M., Hyväluoma, J., 2024. Exploring the RUSLE-based structural sediment connectivity approach for agricultural erosion management. Catena 246, 108420.
Renard, K.G., Foster, G.R., Yoder, D.C., McCool, D.K., 1994. RUSLE revisited: status, questions, answers, and the future. J. Soil Water Conserv. 49 (3), 213–220.
Renard, K.G., Foster, G.R., Weesies, G.A., McCool, D.K., Yoder, D.C., 1997. Predicting soil Erosion by water: A guide to conservation planning with the revised universal soil loss equation (RUSLE). Handbook #703. U.S. Department of Agriculture, Washington, D.C.
Reneau, S.L., Katzman, D., Kuyumjian, G.A., Lavine, A., Malmon, D.V., 2007. Sediment delivery after a wildfire. Geology 35 (2), 151–154. https://doi.org/10.1130/G23288A.1.
Rodrigues, M., de la Riva, J., Domingo, D., Lamelas, T., Ibarra, P., Hoffrén, R., García-Martín, A., 2024. An empirical assessment of the potential of post-fire recovery of tree-forest communities in Mediterranean environments. For. Ecol. Manag. 552, 121587.
Ruffault, J., Limousin, J.M., Pimont, F., Dupuy, J.L., De Càceres, M., Cochard, H., Martin-StPaul, N., 2023. Plant hydraulic modelling of leaf and canopy fuel moisture content reveals increasing vulnerability of a Mediterranean forest to wildfires under extreme drought. New Phytol. 237 (4), 1256–1269.
Sánchez-Benítez, A., García-Herrera, R., Barriopedro, D., Sousa, P.M., Trigo, R.M., 2018. June 2017: the earliest European summer mega-heatwave of reanalysis period. Geophys. Res. Lett. 45 (4), 1955–1962.
Santana, D.B., Lense, G.H., Rubira, F.G., Ayer, J.E., Mincato, R.L., 2024. Serra da Canastra National Park: influence of forest fires on the RUSLE C factor and its impact on water erosion. Notulae Botanicae Horti Agrobotanici Cluj-Napoca 52 (1), 13577.
Shakesby, R.A., 2011. Post-wildfire soil erosion in the Mediterranean: review and future research directions. Earth Sci. Rev. 105, 71–100. https://doi.org/10.1016/j.earscirev.2011.01.001.
Sharp, R., Tallis, H.T., Ricketts, T., Guerry, A.D., Wood, S.A., Chaplin-Kramer, R., Douglass, J., 2015. InVEST 3.2. 0 user's guide. The natural capital project, p. 133.
Shi, C., Liang, Y., Qin, W., Ding, L., Cao, W., Zhang, M., Zhang, Q., 2025. Review of sediment connectivity: conceptual connotations, characterization indicators, and their relationships with soil erosion and sediment yield. Earth Sci. Rev 264, 105091. https://doi.org/10.1016/j.earscirev.2025.105091.
Swarnkar, S., Malini, A., Tripathi, S., Sinha, R., 2018. Assessment of uncertainties in soil erosion and sediment yield estimates at ungauged basins: an application to the Garra River basin, India. Hydrol. Earth Syst. Sci. 22 (4), 2471–2485. https://doi.org/10.5194/hess-22-2471-2018.
Turco, M., von Hardenberg, J., AghaKouchak, A., Llasat, M.C., Provenzale, A., Trigo, R.M., 2017. On the key role of droughts in the dynamics of summer fires in Mediterranean Europe. Sci. Rep. 7 (1), 81.
van der Grift, S., 2021. The Effect of Wildfires on Sediment Connectivity Using the AIC Method – Long Term Analysis for the Águeda Catchment in Portugal from 1979 until 2019. MSc Thesis – Master of Science in Earth and Environment at Wageningen University, The Netherlands.
Verheijen, F.G.A., Jones, R.J.A., Rickson, R.J., Smith, C.J., 2009. Tolerable versus actual soil erosion rates in Europe. Earth Sci. Rev. 94 (1–4), 23–38. https://doi.org/10.1016/j.earscirev.2009.02.003.
Viedma, O., Chico, F., Fernández, J.J., Madrigal, C., Safford, H.D., Moreno, J.M., 2020. Disentangling the role of prefire vegetation vs. burning conditions on fire severity in a large forest fire in SE Spain. Remote Sens. Environ. 247, 111891.
Vieira, D.C.S., Malvar, M.C., Martins, M.A.S., Serpa, D., Keizer, J.J., 2018. Key factors controlling the post-fire hydrological and erosive response at micro-plot scale in a recently burned Mediterranean forest. Geomorphology 319, 161–173.
Vieira, D.C.S., Borrelli, P., Jahanianfard, D., Benali, A., Scarpa, S., Panagos, P., 2023. Wildfires in Europe: burned soils require attention. Environ. Res. 217, 114936.
Vigiak, O., Borselli, L., Newham, L.T.H., McInnes, J., Roberts, A.M., 2012. Comparison of conceptual landscape metrics to define hillslope-scale sediment delivery ratio. Geomorphology 138 (1), 74–88. https://doi.org/10.1016/j.geomorph.2011.08.026.
Wang, Y., Zhou, K., 2023. Effect of slope on the frequency and height of fire whirls. Fire 6 (5), 189.
Wang, H.H., Finney, M.A., Song, Z.L., Wang, Z.S., Li, X.C., 2021. Ecological techniques for wildfire mitigation: two distinct fuelbreak approaches and their fusion. For. Ecol. Manag. 495, 119376.
Wilkinson, S.N., Wallbrink, P.J., Hancock, G.J., Blake, W.H., Shakesby, R.A., Doerr, S.H., 2009. Fallout radionuclide tracers identify a switch in sediment sources and transport-limited sediment yield following wildfire in a eucalypt forest. Geomorphology 110 (3–4), 140–151.
Wu, L., Liu, X., Ma, X.Y., 2018. Research progress on the watershed sediment delivery ratio. Int. J. Environ. Stud. 75 (4), 565–579.
Wu, J., Baartman, J.E., Nunes, J.P., 2021. Comparing the impacts of wildfire and meteorological variability on hydrological and erosion responses in a Mediterranean catchment. Land Degrad. Dev. 32 (2), 640–653.
Wu, Z., Baartman, J.E.M., Nunes, J.P., López-Vicente, M., 2023. Intra-annual sediment dynamic assessment in the Wei River basin, China, using the AIC functional-structural connectivity index. Ecol. Indic. 146, 109775.
Wu, Z., Baartman, J.E.M., Nunes, J.P., López-Vicente, M., 2025. Evaluation of sediment connectivity indices to improve the prediction of the spatiotemporal variability of sediment yield for a large river basin (Wei River, China). Land Degrad. Dev. https://doi.org/10.1002/ldr.70318. In press.
Yang, Y., Hu, X., Han, M., He, K., Liu, B., Jin, T., Huang, J., 2022. Post-fire temporal trends in soil properties and revegetation: insights from different wildfire severities in the Hengduan Mountains, Southwestern China. Catena 213, 106160.
Yang, X., Young, J., Shi, H., Zhu, Q., Pulsford, I., Chapman, G., Moore, L., Gormley, A.G., Thackway, R., Shepherd, T., 2024. Estimating sediment delivery ratio using the RUSLE-IC-SDR approach at a complex landscape: a case study at the lower Snowy River area, Australia. J. Hydrol. 645, 132237.
Yu, M., Bishop, T.F., Van Ogtrop, F.F., 2019. Assessment of the decadal impact of wildfire on water quality in forested catchments. Water 11 (3), 533.